



Norwegian University
of Life Sciences

Master's Thesis 2017 30 ECTS
Faculty of Science and Technology

Design and Control of a Loader Mechanism for the NMBU Agricultural Robot

Erling Fyksen Bjurbeck
Mechanical Engineering and Product Development

Preface

Before you lies the master's thesis concerning the development of a robot arm designed to lift strawberry crates onto the agricultural robot Thorvald II. It has been written to fulfill the graduation requirements for a master's degree in Mechanical Engineering and Product Development at the Norwegian University of Life Sciences (NMBU).

I joined the Robotics and Control group at NMBU in January 2016 to contribute in the development of the agricultural robot Thorvald II. I was eager to participate in a research project where I could use my engineering skills and interest for agriculture while learning about robotics. The engagement led to a summer job at the university where we build the first prototype of the robot. During the summer, the group participated on agricultural events and discussed the application of robotics with farmers. During a visit at Myhrene Gård the initial discussions around what turned out to be the subject of this thesis took place. The initial work on the thesis started with a preliminary feasibility study September 2016.

The period of writing this thesis was kicked off with a trip to Brazil with the other master students of the group. We visited the robotic laboratories of mining company Vale and the Federal University of Rio de Janeiro. We also visited a sugar cane farm producing bio-ethanol and discussed how they could use robots in their enormous fields.

In February 2017 we were selected as the winning group out of twelve participants in the student competition on future agricultural technology at SIMA Paris International Agribusiness Show. We disassembled the prototype robot, laid it in the back of a car, and drove to France where we got present Thorvald to farmers and agricultural companies from all around the world.

Back in Norway, the process of designing the arm and writing this thesis begun. During a few hectic month's I have learned some of the do and don'ts of writing a master's thesis. I hope the contents will enlighten the reader and be a foundation for the future development of the robot arm.

I would like to thank my supervisor Professor Pål Johan From for his supervision and giving me the opportunity to continue the work of this thesis after the submission and hopefully bring it to life. Thanks to Lars Grimstad and Marco Fernades Xaud for helping me with subjects of robotics. Special thanks to Magnhild Skattebu for helping me improve my academic writing, and her efforts with copy editing and motivational support.

Ås
12th of May 2017

Erling Fyksen Bjurbeck

Sammendrag

Til tross for den stadige utviklingen av ny teknologi spiller manuelt arbeid fortsatt en stor rolle i moderne landbruk, særlig i innhøsting. På grunn av den store arbeidskraften som trengs er det en stadig større etterspørsel etter nye maskiner som kan redusere behovet for manuelt arbeid for å redusere utgifter og effektivisere gårdsbruk på en bærekraftig måte.

Denne masteroppgaven omhandler det mekaniske designet og reguleringssystemet til en robotarm laget for å kunne erstatte arbeidere i oppgaver tilknyttet logistikk ved innhøsting av jordbær. Dette gjøres ved at armen løfter kasser med bær opp på en robotplattform som transporterer kassene fra jordet og til et pakkeri. Robotarmen er da montert opp på plattformen. Siden oppgaven er tilknyttet et forskningsprosjekt i landbruksrobotikk ved Norges miljø- og biovitenskapelige universitet, var det naturlig å velge den universitetets robot Thorvald II som plattform.

Oppgaven er delt i to, hvorav Del I omhandler det mekaniske designet av robotarmen, mens Del II skisserer et reguleringssystem for den. Utviklingsprosessen har bestått i å evaluere tilgjengelige løsninger og deretter velge komponenter basert på regulerbarhet, mekaniske egenskaper og kostnader. Valgene som er tatt i Del II er derimot basert på å finne komponenter som er kompatible med robotplattformens nettverk og operativsystem.

Del I: Design og mekanikk

Utviklingen av designet som blir presentert i Del I startet med et forprosjekt gjennomført av Erling Bjurbeck i september 2016. Etter evaluering av forprosjektet ble robotarmen designet for å ha to frihetsgrader og bevege seg i xz -planet. Når armen er montert på robotplattformen vil plattformen bidra med bevegelse i x og y -retning og kunne rotere om z -aksen. Armen er sammensatt av to parallelle ledd laget av rektangulære aluminiumsrør med et rotasjonledd og ett lineært ledd. Begge leddene blir drevet av LinAK LA36 elektriske lineæraktuatorer.

På enden av robotarmen sitter en griper som er designet slik at den omslutter håndtakene på jordbærkassa. Griperen tilpasser seg orienteringen og posisjonen til kassen når den blir plukket opp, slik at den nødvendige presisjonen til robotarmen er redusert. Rammen til griperen er laget av aluminiumsvinkler og -plater. En likestrømsmotor med snekkedrev styrer klørne til griperen via en dobbel stagmekanisme.

Del II: Modellering og regulering

Geometrien til robotarmen blir modellert matematisk og den inverse kinematikken løst analytisk. Kinematikken vil bli brukt senere til implementeringen av en posisjonsbasert reguleringssystem.

To RoboteQ SDC2160 motorkontrollere er valgt til å regulere alle fire motorer i armen. Lineæraktuatorene er regulert i lukket sløyfe, mens likestrømsmotoren reguleres i åpen sløyfe med endebrytere på gripemekanismen. Det ble utført laboratorieforsøk for å pare kontrollerne og motorene. Forsøkene avdekket programvarefeil i kontrolleren og bekreftet at kontrollerne må kjøre et skript for å fungere optimalt.

Masteroppgaven legger grunnlaget som trengs for å bygge en prototype og lage et styringsskript for å teste det mekaniske designet og reguleringssystemet.

Abstract

Despite the development of new technologies, manual labour still continues to play a large role within most modern agricultural operations, especially during harvest. Consequently, there is an increasing demand for new machines to reduce labour as a means to limit costs, while increasing efficiency in a sustainable manner.

This thesis concerns itself with the design of a mechanism and control system for a robot arm that can substitute workers in logistical operations during strawberry harvest. More specifically, by lifting berry crates onto a robot platform and transporting them from the fields and to the packaging facilities. The robot arm is to be mounted on the platform composing a vehicle-manipulator system. As this thesis is connected to a general research project on agricultural robotics at the Norwegian University of Life Sciences, the chosen platform is the associated field robot Thorvald II.

The thesis is divided into two parts, where Part I concerns the mechanical design of the robot arm, while Part II proposes a system for controlling the mechanism. The design development process has involved assessments of available solutions before selecting components on the basis of controllability, mechanical properties and costs. The process of selection in Part II is however, based on finding solutions that are compatible with the robot platform's network (Controller Area Network) and operating system (Robotic Operating System).

Part I: Design and Mechanics

The design of the robot arm presented in this thesis began with a preliminary feasibility study conducted by Bjurbeck in September 2016. Following the assessment of this study, the robot arm is designed to have two degrees of freedom operating in the xz -plane. When mounted on the platform, the arm will be free to operate in a 3-dimensional space, as the platform moves in x and y -direction, and rotates around the z -axis. The arm is assembled from two parallel link pairs made from rectangular aluminium tubes, and a revolute and prismatic joint. Both joints are actuated by LinAk LA36 linear electric actuators.

The end effector of the arm is a gripper head designed to grasp the handles of the strawberry crate. The gripper head is self-aligning with the crate's orientation in order to reduce the precision of control needed to envelop and grasp the crate. The frame of the gripper head is made from aluminium angle profiles and sheet metal. A worm drive DC motor actuates the gripper claws via a double link mechanism.

Part II: Modeling and Control

The geometry of the design presented in Part I is modelled mathematically and the inverse kinematics solved analytically. The kinematics will be used in future implementation of a position control system.

Two RoboteQ SDC2160 dual-channel controllers are chosen to control all four actuator motors. The linear actuators are controlled in closed loop position tracking mode with absolute feedback. The gripper motor is controlled in open loop mode with end stop switches detecting the position of the claws. Experiments were conducted to match the controllers with the actuator motors. The experiments revealed firmware issues with the controller. The experiments also affirmed the controller needs a script to operate the actuators efficiently.

The thesis provides the foundations to build a prototype and write an operating script to test the mechanical design and control system.

List of Tables

1.1	NASAs definition of technology readiness levels [1]	4
1.2	Time factors of workers in strawberry production at Myhrene Gård [2].	7
3.1	Mechanical and physical properties of aluminium alloys and structural steel. Table data from Rørvik [3]	20
3.2	Composition and mechanical properties of a selection of steel alloys. Table data from Callister [4].	21
3.3	Composition and mechanical properties of a selection of aluminium alloys. Table data from Callister [4].	21
4.1	Conceptual selection matrix of the feasibility study [5]	26
4.2	Metric boundaries of the crate loader system's attributes [cm].	33
5.1	Specifications of LinAk's LA36 [6].	37
5.2	Specifications from the data sheet of the worm gear motor.	38
6.1	Part list of figure 6.1.	44
6.2	Part list of figure 6.3	46
7.1	Length of lines in figure 7.1 and 7.2.	67
7.2	Limits of joint variables	70
9.1	Specs of Mean Well DC/DC transformer [7].	76

List of Figures

1	Defined axis of the coordinate system.	xii
1.1	The Thorvald II fleet	3
1.2	Traditional strawberry picking at Myhrene Gård, Sylling, Norway.	4
1.3	(a, d): Two examples of implemented robots in strawberry production. (b, c): Futuristic ideas of robots in strawberry production.	5
2.1	The working principle of a single acting spring return cylinder (top) and a double acting cylinder (bottom). Courtesy of Machine Design [8].	11
2.2	Basic principle of a DC motor: The forces induced between the electromagnetic rotor and the permanent magnets of the stator spins the rotor. Courtesy of Wiki- media Commons [9].	12
2.3	Different types of electric DC motors. Courtesy of Tiger Motor, Thompson, Robot Gear, and Elmo Motor Company [10, 11, 12, 13]	14
2.4	Four types of rotary actuators for robot arm joints.	16
3.1	A variety of tubes and profiles available in steel and aluminium. Courtesy of Robor, PA International [14, 15]	22
3.2	Principle sketch of two joint types. Courtesy of Wikimedia Commons [16, 17]	24
4.1	Sketches of the initial concept alternatives.	25
4.2	Flow diagram of the loader operation.	27
4.3	Illustration of the system's two degrees of freedom, with one revolute and one prismatic joint.	27
4.4	Sketch of a possible layout of the arm actuation.	28
4.5	Concept sketch of the gripper head frame, with a sloped skirt providing self- alignment as the head envelops the crate.	29
4.6	Sketch of a possible layout of the gripper claws.	30
4.7	Simple sketch of the base frame principle.	31
4.8	Row environments at Myhrene Gård.	32
4.9	Metric boundary attributes.	33
5.1	LinAk LA36 [6]	37
5.2	24 V DC motor with worm drive.	38
5.3	Free body diagram of a worst-case scenario of actuator load of the arm.	40
5.4	Free body diagram (i), shear (ii) and moment diagram (iii) of a worst-case scenario of structural loads on the arm.	41
6.1	Part number call-out of the gripper head.	44
6.2	The gripper head holding a strawberry crate.	45
6.3	Part number call-out of the loader.	46
6.4	The complete assembly of the crate loader.	47
6.5	Base frame with the crate bed.	48
6.6	Four brackets of the loader design.	49
6.7	Miscellaneous parts of the gripper head.	50
6.8	Pair of parts of the loader design.	51

6.9	Two examples of platform configurations.	52
6.10	The loader implemented onto the most possible narrow platform configuration.	54
6.11	Rendering of the table-top configuration in it's right environment.	55
6.12	Bird's eye perspective of the loader in motion.	55
6.13	3D rendering of the wide double-row configuration.	56
6.14	Photo manipulation of the robot platform in a double-row environment.	56
6.15	3D rendering of the narrow double-row configuration.	57
7.1	Cosine triangle of the base link actuator setup.	67
7.2	Joint variables of the actuators, d_1 and d_2	68
7.3	Workspace in green between the lines. Collision zones in red.	70
8.1	Block diagram of a basic closed-loop control system.	72
8.2	Basic principle of an absolute rotary encoder. Courtesy of Wiedemann [18]	73
9.1	Architecture of the power and communication system.	75
9.2	Mean Well 19-72V to 24V DC/DC converter. Courtesy of Elfa Distrelec [7]	76
9.3	Roboteq SDC2160. Courtesy of Roboteq [19]	77
9.4	Circuit diagram of the parallel base arm link actuators and controller.	78
9.5	Circuit diagram of the end arm link actuator and the claw motor.	79
9.6	Communication network diagram.	80
10.1	Photo of the workbench in the robotics lab.	82
10.2	Screen-shot of the Roborun+ Utility-program, showing the response of the linear actuator control.	82
10.3	A simple MicroBasic script. Courtesy of Grimstad [20].	84

Abbreviations

CAN Controller Area Network.

FBD Free Body Diagram.

FEA Finite Element Analysis.

IFCO International Fruit Container.

MPC Model Predictive Controllers.

PAC Programmable Automation Controller.

PLC Programmable Logic Controller.

PM Permanent Magnet.

ROS Robotic Operating System.

TRL Technology Readiness Level.

UAV Unmanned Aerial Vehicle.

UGV Unmanned Ground Vehicle.

URDF Unified Robot Description Format.

XML Extensible Markup Language.

Coordinate System

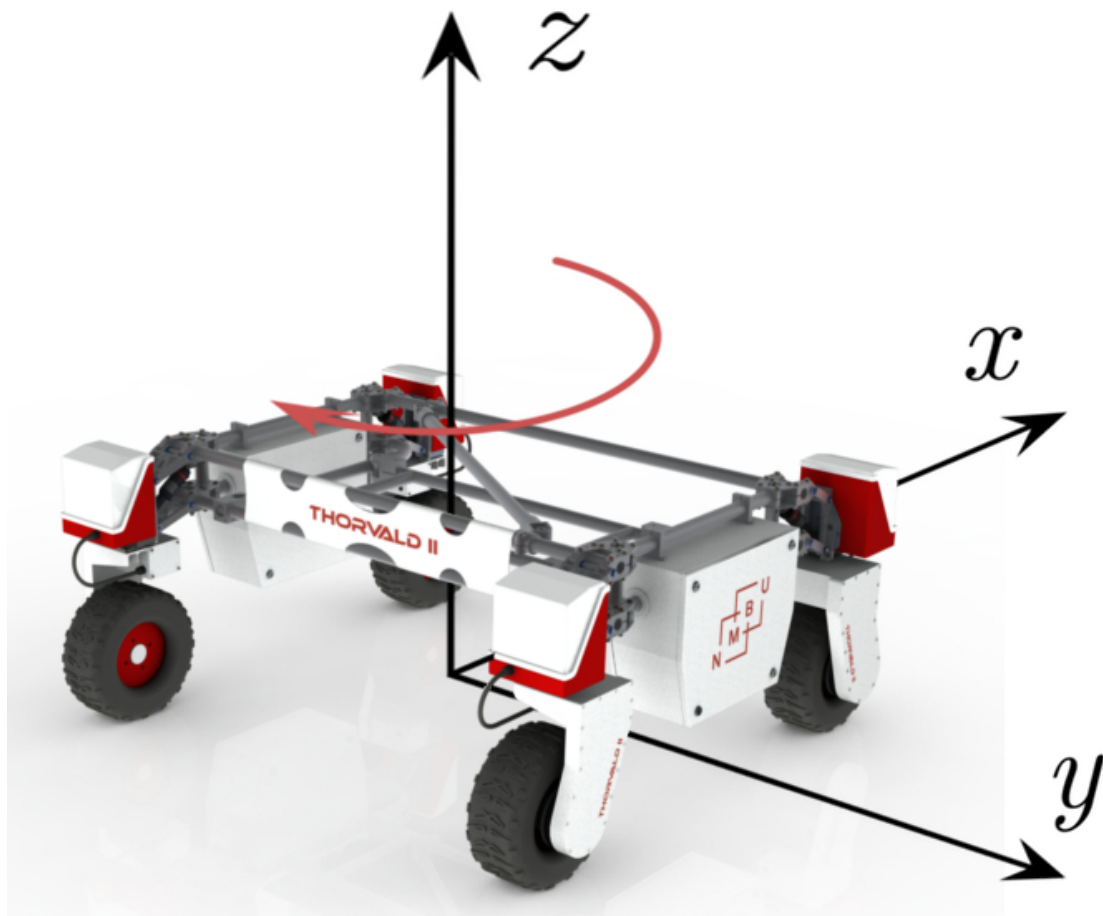


Figure 1: Defined axis of the coordinate system.

Contents

1	Introduction	1
1.1	Background	1
1.1.1	Field Robots and Vehicle-manipulator Systems	2
1.1.2	Thorvald - The Agricultural Robot Project of NMBU	2
1.1.3	Potential in Strawberry Production	3
1.1.4	Technology Readiness Level	3
1.1.5	Feasibility Study	3
1.1.6	State of the Art	5
1.2	Conceptual Requirements	6
1.3	Scope of the Thesis	7
I	Design and Mechanics	9
2	Types of Robot Actuators	10
2.1	Pneumatic Actuator	10
2.2	Hydraulic Actuator	11
2.3	Electric Motors	12
2.3.1	Brushed DC Motor	13
2.3.2	Brushless DC Motor	13
2.3.3	Servo Motor	13
2.3.4	Stepper Motor	13
2.3.5	Linear DC Motor	14
2.4	Linear Electric Actuators	14
2.5	Mechanical Drives In Robotics	15
2.5.1	Timing Belts	15
2.5.2	Bevel Gear	15
2.5.3	Worm Drive	15
2.5.4	Harmonic Drive	16
2.5.5	Direct Drive	17
3	Materials and Mechanics	19
3.1	Material Properties	19
3.2	Metal Alloys	20
3.2.1	Steel	20
3.2.2	Aluminium	20
3.3	Structural Parts	21
3.3.1	Hot and Cold Rolled Steel Profiles	21
3.3.2	Extruded Aluminium Profiles	22
3.4	Material Stress Properties	23
3.5	Joints	23

4	Features and System Design	25
4.1	Conceptual Selection	25
4.2	Basic Functions	26
4.3	Design of the Arm	28
4.4	Design of the Gripper	29
4.4.1	Gripper Frame	29
4.4.2	Gripper Claws	30
4.5	Base Frame	31
4.6	Working Environment	32
4.7	Metric Boundaries	33
5	Component Selection	35
5.1	Actuation Components	35
5.1.1	Actuation of the Arm	36
5.1.2	Actuation of the Gripper	36
5.1.3	Linear Actuator - LinAk LA36	37
5.1.4	Brushed 24 V DC-motor With Worm Drive	38
5.2	Structural Components	39
5.3	Design Verification	39
5.3.1	Actuator Force	40
5.3.2	Structural Capacities	41
6	Assembly and Setups	43
6.1	Gripper Head	44
6.2	Arm Assembly	46
6.3	Base Frame and Crate Bed	48
6.4	Minor Parts of the Assembly	49
6.4.1	Brackets	49
6.4.2	Miscellaneous Parts	50
6.5	Integration and Setups	52
6.5.1	Robot Platform Configurations	52
6.5.2	Table-top Configuration	54
6.5.3	Wide Double-Row Configuration	56
6.5.4	Narrow Double-Row Configuration	57
	Discussion Part I	59
	Conclusion Part I	63
II	Modeling and Control	65
7	Mathematical Modeling	66
7.1	Kinematics	66
7.1.1	System Geometry	67
7.1.2	Forward Kinematics	68
7.1.3	Inverse Kinematics	69
7.2	Workspace	70
8	Controlling the Loader	71
8.1	Closed Loop Control System	71
8.2	PID Controller	72
8.3	Absolute Encoder	72
8.4	Controller Area Network	73
8.5	ROS: Robotic Operating System	73

9 Architecture	75
9.1 Power Transformation	76
9.2 Motor Controller - Roboteq SDC2160	77
9.3 Power Circuit	77
9.4 CAN and ROS Integration	79
9.5 Loader Position Control	79
9.6 Gripper Control	80
9.7 Safety	80
10 Control Setup	81
10.1 Controller Setup	81
10.2 Actuator Control Loop	83
10.3 Gripper Control Loop	83
10.4 Programming the Controllers	84
10.5 Operating Script	84
Discussion Part II	85
Conclusion Part II	86
Future Work	87

Chapter 1

Introduction

This is a master's thesis intersecting mechanical engineering, product development and robotics. The thesis is connected to what is assumed to be the world's largest research project in agricultural robotics focusing on developing new farming technologies, and increasing agricultural production in a sustainable manner.

The goal of the thesis is to design an implement enabling the agricultural robot Thorvald II to perform logistical tasks relating to strawberry harvest.

1.1 Background

The agricultural business is facing a comprehensive changeover in terms of production methods and employment. Although modern industrial agriculture is high tech, a wide range of task still continues to be manually conducted. The declining availability of farm workers and the cost of labour has been and continues to be a huge challenge for farmers. As a result, farmers in most developed countries rely on seasonal immigrant workers. The cost of labour and the increased demand for profit push farmers and researchers to come up with new technological solutions to increase agricultural productivity and efficiency. The increased use of greenhouses, digital farming, and automation of the agricultural industry opens the door for a change of paradigm.

Aside from the increased use of automated vehicle guidance in the fields, automation today is mostly restricted to permanent installations like greenhouses, livestock buildings and packaging facilities. Tasks that require near flawless perception, harvest, and handling of fragile produce in the field are usually done manually. The production of high value crops (fruits and greens), strawberries in particular, is still dominated by manual labour.

One of the fastest developing fields in agricultural technology is the utilization of robots. The term agricultural robots may include unmanned aerial or ground vehicles (UAVs or UGVs), driverless tractors, greenhouse- and milking robots. Small or airborne robots can perform surveillance and measure properties of soil, crops, and even herd animals. Larger terrestrial robots are applicable to more power demanding tasks like weeding, spraying, sowing, harvest, and logistics.

Milking robots and other robots associated with livestock facilities has been around for some time. However, it is difficult to substitute humans with machines in many of the complex farming tasks. Matching the dexterity of humans, for instance, is one of the biggest challenges in robotics. Many established and startup agricultural technology companies are

therefore developing new innovative robotic solutions to take on the future of farming. Yet the market for the advances of the sector suffer from fragmented development, insufficient robotic solutions, poor administrative support and issues on infrastructure.

The future of agricultural robotics is promising despite its market challenges. This assumption is supported by a report from the market intelligence firm Tractica which suggests that sales of agricultural robots in general will reach around 600,000 units annually by 2024 [21]. The report also estimate the international market to reach \$ 74 billion in annual revenue.

1.1.1 Field Robots and Vehicle-manipulator Systems

Despite the booming research on mobile agricultural field robots there is no known research project on utilizing robots in farming logistics outside greenhouses.

Enabling field robots to contribute in farming logistics requires the mobile robot platform to have the ability of handling, loading, and unloading objects. Robots that manipulate and handle objects has over the last decades become a robust and well developed technology. Robotic arms are today used extensively in many modern industries. However, the use of robot manipulators has been restricted to structured environments like factory floors. New technology on machine vision, autonomy and mobile robots enables the possibility of bringing the technology of robotics outdoors. Allowing a system with the capabilities of a robot manipulator to move around in their environment freely, will open doors for new areas of robotic application. Robots of this character are called vehicle-manipulator systems.

The use of vehicle-manipulator systems in agriculture automation is a promising research area [22]. The repetitive tasks of farming and the extensive field areas makes vehicle-manipulator systems very applicable to agriculture. Agricultural robot platforms are usually wheel driven, tractor-like vehicles that operate autonomously in the fields. While the robot moves around, the manipulator can perform tasks like harvesting, sample-taking etc.. The tasks are, however, constrained by the limited lifting capacities of the manipulators used in such systems.

1.1.2 Thorvald - The Agricultural Robot Project of NMBU

The initial idea of the agricultural robot platform discussed in this thesis came to life at the Norwegian University of Life Sciences (NMBU) in 2014. A group of five students supervised by Professor Pål Johan From designed and built the first prototype of a low-cost lightweight multipurpose field robot, named after the university's prime student: Thorvald.

Since then, the project has evolved into an international collaboration between NMBU and the University of Lincoln with several industrial partners. The collaboration coordinated by Prof. From is considered by the Financial Times to be the world's largest research project in agricultural robotics [23] with over 30 full-time researchers and numerous master students.

In 2016, the project's startup company SAGA Robotics and the student group NMBU Robotics and Control built a second prototype designed by the master students Sund and Austad [24, 25]. A new modular concept and industrial design constitute the next generation robot: Thorvald II. The modularity of the concept enables a wide range of configurations to be assembled from the same basic parts, as illustrated in figure 1.1. The design of Thorvald II is currently under further development for serial production by the end of 2017.

In February 2017 the Robotics and Control group at NMBU participated in the student competition at SIMA Paris International Agribusiness Show. As the only project out of 12

participants, the group was granted a presentation stand and had live demonstrations of the robot. The response from farmers and researchers from all around the world encourages and builds optimism for the future of the project.



Figure 1.1: The Thorvald II fleet

1.1.3 Potential in Strawberry Production

The robot project is in collaboration with farmer Simen Myhre at Myhre Gård (farm) in Sylling. Myhre is Norway's second biggest strawberry farm, with a correspondingly large workforce. During a visit with the NMBU Robotics and Control group in June, 2016, Myhre informs that the strawberry-picking workers on average spend 40 % of their time on quality control, transportation and weighing crates. This accounts for over 2 million NOK in wages during one season. Myhre addressed the issue and suggested to utilize Thorvald in logistics during harvest.

1.1.4 Technology Readiness Level

The technology readiness level scale (table 1.1) is a planning tool for innovation management, developed by the National Aeronautics and Space Administration (NASA) in the 1970's. NASA presented the scale as a tool to allow for a more effective assessment of, and communication concerning the maturity of new technologies [26]. The scale is used in this thesis to manifest the goals and different steps throughout the project process.

1.1.5 Feasibility Study

A preliminary feasibility study (Bjurbeck [5]) for this thesis was carried out by the author during the fall of 2016. The goal of the study was to evaluate different concepts and design



Figure 1.2: Traditional strawberry picking at Myhrene Gård, Sylling, Norway.

Table 1.1: NASA's definition of technology readiness levels [1]

TRL Scale	Description
TRL 1	Basic principles observed and reported
TRL 2	Technology concept or application formulated
TRL 3	Analytic and experimental proof of concept
TRL 4	Component/subsystem validation in laboratory
TRL 5	System/subsystem/component validated in relevant environment
TRL 6	Prototype demonstrated in relevant environment
TRL 7	System prototyping demonstration in operational environment
TRL 8	Actual system completed and mission qualified
TRL 9	Actual system mission proven in operational environment

options of an implement to enable the robot platform Thorvald II to handle logistics in strawberry production. The study discussed the main concept, features, and basic principles of a crate loader mechanism. It finally suggested the mechanical design of a simple robot arm operating in the xz -plane with one degree of freedom. The study also evaluated a design with two-DOF and briefly discussed possible actuation methods. By observing and reporting the basic principles and further formulating the concept and application, the project was brought up through level 1 and 2 on the TRL scale (table 1.1).

One of the early conclusions of the study was the advantages of minimizing the number of degrees of freedom. Fewer DOFs reduce the mechanical complexity and simplifies control. However, the suggested arm design with only one degree of freedom could not perform all of the required functions.

The study evaluated material and components that will be further assessed in this thesis. There study was limited to mechanical design and did no assessment of control components or methods. Thus, it is only relevant for Part I of the thesis.

The concept of the crate loader was validated through external trial by discussions with

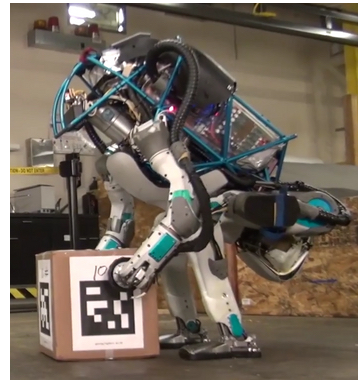
a group of experts. This made it safe to continue the development of the design through this thesis. The conclusions and assessments of the study is further elaborated in section 4.1.

1.1.6 State of the Art

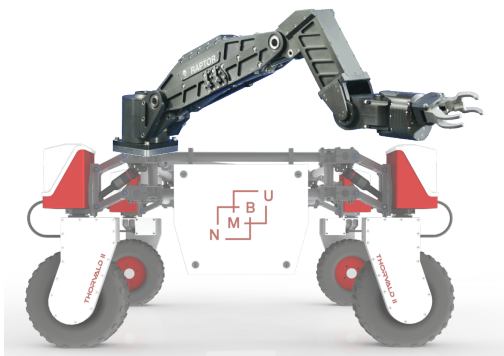
There is no known crate handling field robot on the market today. There are, however, several robots that can perform some of the tasks involved separately.



(a) The Agrobot platform [27]



(b) Boston Dynamics' Atlas humanoid robot [28]



(c) An industrial robot manipulator photo-shopped onto Thorvald II



(d) The green house based picking robot Berry Nice [29]

Figure 1.3: (a, d): Two examples of implemented robots in strawberry production. (b, c): Futuristic ideas of robots in strawberry production.

The SW6010 by Agrobot (figure 1.3a) is an autonomous harvesting robot for strawberries in prepared fields. A system of stereocameras and a color analysis program recognizes ripe berries and feeds their position to a set of manipulators that picks the berries [27]. Although the harvesting process is autonomous, quality control, packaging, and crate handling remain manual. The robot has a tractor chassis and is driven by an operator. To a small degree the SW6010 reduces time spent carrying crates, but the unloading is still done by hand.

The robot is not adapted for use in Norwegian fields (open land rows), as it only operates in fields with specifically arranged rows with plastic walls.

In the endeavor of substitute workers with humanoid robots, Boston Dynamics sets a benchmark of the industry with their Atlas robot (figure 1.3b). This agile anthropomorphic robot is design to have high mobility in rough terrain, with arms free to lift and manipulate objects such as crates [28]. However, the Atlas is a highly sophisticated robot primarily designed for defense purposes, and its high price makes it unsuitable for the Norwegian agricultural scene.

Over the last half century, robotic arms has become a well developed technology with a wide range of applications. Although many pick-and-place manipulators of all sizes and prices are available on the market, these are primarily designed to be stationary. Consequently, they have high weight relative to their lifting capacity. This makes typical industrial arms (figure 1.3c) inconvenient to implement onto the Thorvald-platform.

In 2011, the Japanese company Shibuya Seiki presented their strawberry-picking greenhouse robot Berry Nice (figure 1.3d). The autonomous picker robot utilizes similar vision technology as the SW6010, and is designed to operate on rails in greenhouses. The berries are loaded into an onboard tray which is discharged to a tray stocker [29]. The trays are transported on a system of rails to the handling facility in the automated operation environment.

1.2 Conceptual Requirements

The performance requirements of the robot system is based on the operational efficiency of human workers (table 1.2) and the physical environment of the strawberry fields and poly-tunnels. Nonetheless, robots does not necessarily have to work faster than the humans, as long as their operation is satisfactory. Most importantly, the system aims at reducing the labor needed to transport the berries from the pickers hands to the packaging facility.

There are several aspects of importance in the system design. Firstly, the crates in which the berries are picked can not touch the soil, as it may cause mildew and contamination of the berries. In order to prevent this, the crate are either stacked upon an empty crate or placed on a two-wheeled dolly during conventional harvest. However, Myhre informs that legged crates that prevent soil contact are available on the market. Secondly, crates must be handles with delicate care and gentle motion in order to protect berries from impact damage. Thirdly, berries has to be cooled rapidly after picking in order to prevent quality loss. Maintaining the required time interval between picking and cooling will most likely be the ultimate factor in determining the efficiency of the system. Besides carrying the crates, workers must control the weight of the crate and each tray, and do a visual quality inspecting before handing over the crates for warehouse transportation. Weighting of the smaller trays in the crate and quality control would still have to be carried out manually. Finally, a great factor of the system design is the human-robot interaction. For instance, the robot could work as a slave to the human picker, follow along, or be deployed for transport missions. Or, the robot could work independently by picking up and transporting crates left behind by the pickers. The latter allows the robot to work more efficiently, and was therefore chosen as the basis of the concept.

The physical environment regarding robot and implement configuration will be further elaborated in chapter 6. Myhre suggests that in a 10 to 15 year perspective, open land double rows will be the preferred environment until table top production takes over.

Table 1.2: Time factors of workers in strawberry production at Myhre Gård [2].

Average time spent picking one crate of berries	15 min
Average time spent carrying, weighting and controlling one crate	10 min
Max. time from picking to packing facility	60 min

1.3 Scope of the Thesis

The purpose of this thesis is to further develop the prototype design of an implement for loading IFCO crates onto the field robot Thorvald II. The design process involves selecting components and designing mechanical parts and the complete assembly of the implement. The process also includes designing the architecture of the control system, and preparing it for integration with the operating framework of the robot platform.

Part I: Design and Mechanics

The design is based on the findings of the project's feasibility study. With the study as a basis, the thesis aims to refine the conceptual idea of the implement and present thoroughly assessed components and design solutions. Modularity and the use of catalogue items has to be pursued to ensure rapid construction and to keep costs low. This should, however, not compromise the performance of the system.

Part II: Modeling and Control

The design presented in Part I is modelled mathematically in order to control the position of the loader from actuator feedback and conducting a workspace analysis. The architecture of the control system will be presented subsequently. The thesis also aims to form the basis for writing an operating script and prepare the implementation of the control system on the operating system of the robot platform.

Developing the design and control of the loader mechanism is one of many steps on the way to create a complete autonomous crate handling field robot. The subjects of further development, such as machine vision, object recognition, robot positioning and control algorithms, is however left out in order to constrain the scope of the thesis.

The associated research of this thesis was granted financial support from The Research Council of Norway through the "Småforsk"-initiative at NMBU. The grant serves as the main budget for the prototype design and the procurement of components must therefore be restricted accordingly.

The thesis will not document the manufacturing process and testing of the initial prototype. As a consequence, the project will not be able to climb to the fourth level of the TRL-scale within the time frame of this thesis submission. The final goal of the thesis is therefore set to present analytic and experimental proof of both the design and control part of the concept.

Product development goal:

Raise the concept from stage 2 up to 3 on the TRL scale.

Part I

Design and Mechanics

Chapter 2

Types of Robot Actuators

An actuator is an electromechanical device that connects the electronic signal from a processor to the actual mechanical motion [30]. The work of the actuator can both induce or object a motion, and operate in both linear and rotational directions. A linear actuator evidently creates a linear motion, but can be driven by a rotational motion, e.g. a simple DC motor. Likewise, a rotational actuator can be driven by a linear motion to create rotational motion, like a crank and slider.

With new development, the science of actuation is a growing field. Some inventions include flexible actuators like hydraulic artificial muscles and shape memory alloys, while there also are electric solenoids and micrometer precise piezo-electric actuators available on the market [31]. The following section only describes the actuator types of interest within the force-requirements of the thesis.

2.1 Pneumatic Actuator

Pneumatic actuators can be used to create linear and rotational motion. The basic design is built up by a piston inside a hollow cylinder. Compressed air flows in and pushes the piston, as shown in figure 2.1. The first advantage of pneumatic actuators are found in their simplicity and few moving parts. Depending on the bore size and air pressure, the available forces range from 100 N to 200 kN [8]. Moreover, pneumatics can be used in environments with extreme temperatures of -40 to 120 °C. Concerning safety, pneumatic actuators hold further advantages as they operate without hazardous fluids or electric sparks. They thereby comply with explosion proof ratings and machine safety requirements. Pneumatic systems are also suitable for installation in tight compartments and are regarded as a cost-efficient alternative in linear motion.

There are, however, many disadvantages in pneumatic actuators. Pressure loss and the compression of air cause general low efficiency. The system needs a compressor running constantly in order to maintain air pressure. Pneumatic cylinders are most often designed to perform very specific tasks, and should be strictly purpose designed. The actuators must have regulators and valves in order to enable precise control. This will in turn complicate design and raise the costs. Pneumatic systems are also facing issues of air contamination, as well as maintenance of fluid lines and the compressor.

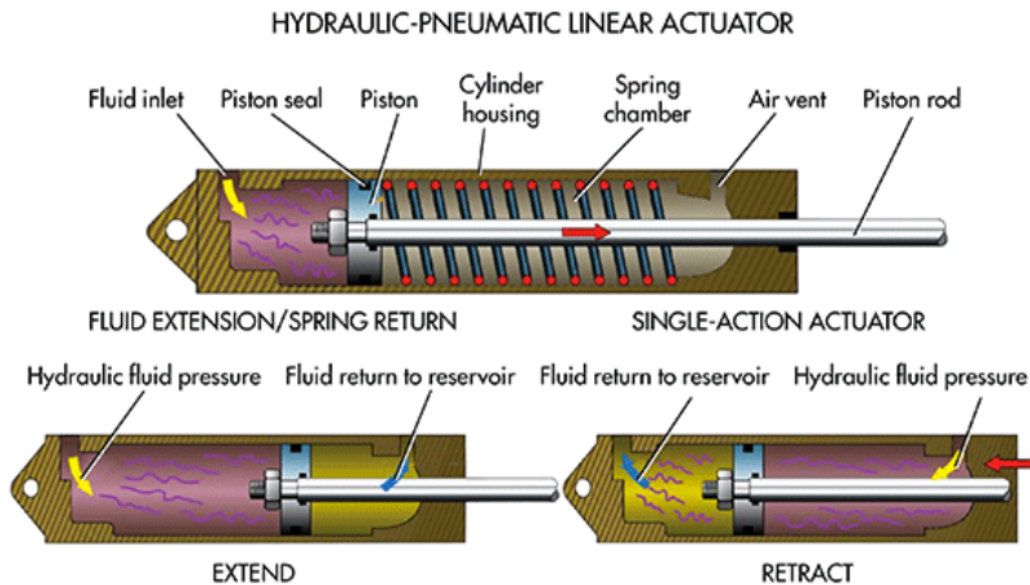


Figure 2.1: The working principle of a single acting spring return cylinder (top) and a double acting cylinder (bottom). Courtesy of Machine Design [8].

2.2 Hydraulic Actuator

Hydraulic actuators follow the same working principle of pneumatic actuators, but utilize an in-compressible fluid instead of air. According to Pascal's law [32], when there is an increase in pressure at any point in a confined fluid, there is an equal increase at every other point in the container. Considering this and the properties of in-compressible fluids, the forces available in hydraulic systems can be 25 times higher than in pneumatic systems [8]. Although hydraulic cylinder housings normally are bigger, the force-to-weight ratio remain higher than in pneumatic cylinders. Hydraulic actuators also have the capacity of holding forces when the pump is turned off. Similar to pneumatic systems, hydraulic actuators keep their pumps separated from the actuator.

Many of the disadvantages of hydraulic actuators systems are similar to those of pneumatic ones. Hydraulic systems require a pump with motor, fluid reservoir, heat exchangers, valves, and lines. Most of these parts are of considerable sizes and are mainly designed to exert large forces. Any hydraulic system will also leak fluid, which may reduce efficiency and harm the environment.

2.3 Electric Motors

An electric motor is a machine that converts electric energy into mechanical energy. Electric motors can range in size from a single molecule [33] to enormous 101 MW wind tunnel-motors [34], and is therefore found in an infinite number of applications like trains, cars, pumps etc.. Electric motors are the most common actuator type in robotics [31].

The principle of electric motors is based on electromagnetism. An electric motor is mainly made up of a stator and a rotor, respectively a stationary and a rotating component. As seen in figure 2.2, the rotor generally has electromagnets and the stator has permanent magnets. However, the configuration may also be the other way around. When currents run through the windings of the rotor, the magnetic field induce magnetic forces between the rotor and the stator. These forces make the rotor and stator poles attract and repulse (red and blue arrows in figure 2.2), consequently turning the rotor.

Alternating current motors have traditionally been used in industrial applications, since electric utility systems provide alternating current. In mobile robots, however, direct current is preferable. Firstly, the torque and speed-characteristics of the DC motor have a wide range and a high efficiency [35]. Secondly, the circuits of all robot are direct current. Finally, mobile robotic systems store energy in batteries, which rules out the use of alternating current.

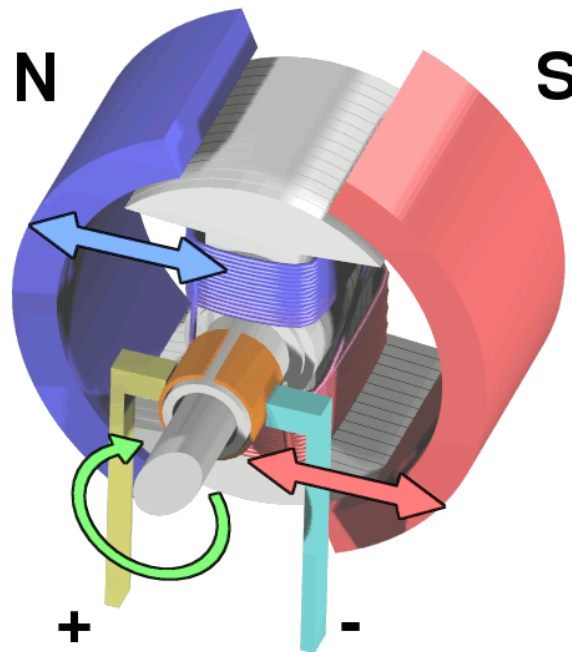


Figure 2.2: Basic principle of a DC motor: The forces induced between the electromagnetic rotor and the permanent magnets of the stator spins the rotor. Courtesy of Wikimedia Commons [9].

2.3.1 Brushed DC Motor

Brushed DC motors are the classical example of an electric motor. The brushed motor has permanent magnets in the rotor while the stator has electromagnets, contrary to the motor in figure 2.2. In order to detect the direction of rotation, the brushes touching the rotor shaft are used as a commutator (in fig. 2.2: yellow and blue leads touching the orange field on the shaft). To enable rotation using direct current, the commutator detects the change in orientation and flips the current so that the rotation continues. Naturally, the flipping is not needed in alternating current motors. Brushed DC motors has a wide speed range but they produce a meager torque, often making them inadequate in robotics. The lack of torque can, however, be compensated for with gears.

2.3.2 Brushless DC Motor

Similar to the brushed motor, a brushless motor (figure 2.3a) also has permanent magnets in the rotor and electromagnets in the stator. Because they are brushless, these motors have no way of flipping the current in order to maintain rotation. Therefore, they depend on encoders or sensors to measure rotation [31]. Brushless motors are well suited for robots as they deliver greater torque and speeds than brushed motors. However, due to the complex design and need of controllers they are more expensive than brushed motors.

2.3.3 Servo Motor

The term servomotor (figure 2.3d) applies to a motor system that uses feedback signals to control the position and motion of the output shaft. A motor of choice is coupled to an encoder that measure the position before sending the signal back to a controller. From the programmable position controller, the input signal is processed through a servo control, which amplify the signal to a level that affects the motor. As the motor turns, a new signal from the encoder is continuously fed back to the position controller. This signal is then used to further control the motor towards the desired input value [36]. From the change in position, the controller can derive both speed and acceleration. This control system allows the system to be brought to the desired positions with a programmed behavior. Servo motors are therefore highly relevant in robotic applications. A more elaborate description of control systems will be presented in chapter 8.

2.3.4 Stepper Motor

Step motors (figure 2.3c) are actuators that convert a digital input into an analog motion. Steppers move in angular increments of equal magnitude depending on the motor type. Consequently, stepper motors operate in separate angular increments instead of one continuous motion. As a result, step motors are convenient when the controller uses pulse signals, where one pulse equals one increment of motion. Step motors consume power to hold the desired position, whereas a servo motor rests. Steppers also are a simpler alternative to servomotors, but are limited to powers under 1 kW and speeds of 2000 rpm [36]. Stepper motors are therefore best suited in lightweight applications in the scene of mobile robotics.

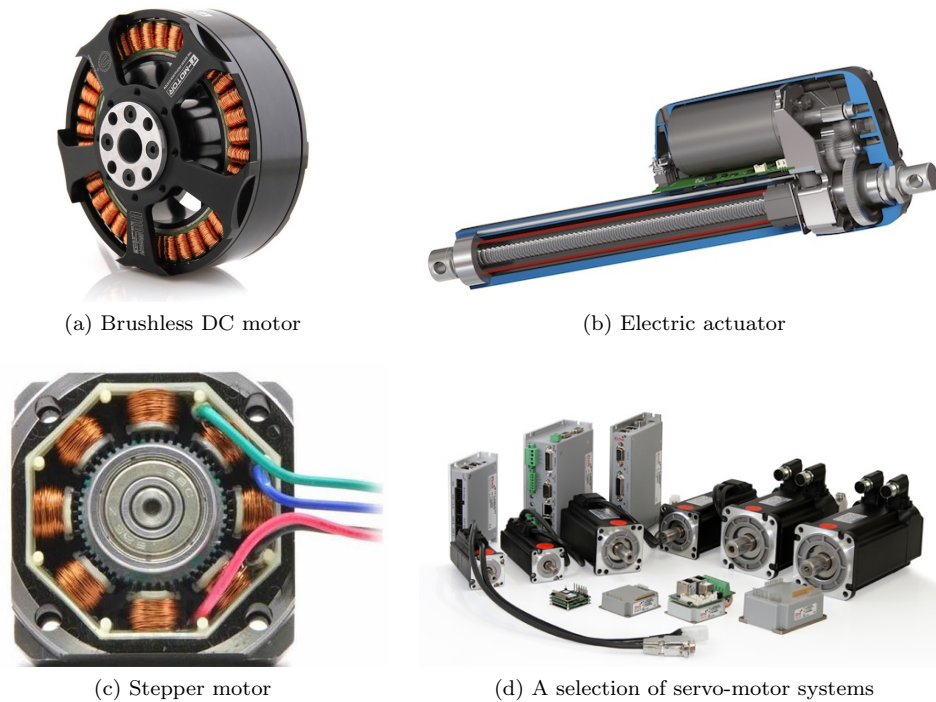


Figure 2.3: Different types of electric DC motors. Courtesy of Tiger Motor, Thompson, Robot Gear, and Elmo Motor Company [10, 11, 12, 13]

2.3.5 Linear DC Motor

Electric linear DC motors are in essence a DC motor with its stator wrapped out and put flat [31]. Linear motors are ideal for installations that require high speeds and rapid acceleration, as there are few and small parts, no gearing, and low friction. Linear motors therefore have a long operational life. The force output of linear motors are generally low. The current draw is also high relative to the force exerted [37]. Furthermore, the linear motors' sliders runs on a guide or rail that needs protection against fluids and debris.

Further descriptions on the basic principles of electric motors can be found in Wildi's *Electric Machines, Drives, and Power Systems* [35].

2.4 Linear Electric Actuators

Self contained linear actuators (figure 2.3b) are a compact alternative to pneumatic or hydraulic actuators as they incorporate the motor, drive and position sensor in one unit. The design yields a high force-to-volume ratio compared to the above-mentioned alternatives. The spindle drive allows both self-locking and free running capabilities [37]. Actuators are generally available with a wide range of gear ratios and spindle pitches, which in turn yield low output speed. Although spindle actuators are most common, belt driven units are also available. Most electric linear actuators are powered by a brushed DC motor with an

encoder or a feedback potentiometer. While DC motors are highly efficient they also enable superior feedback control options, with precise positioning, networking and programmable motion profiles [8]. However, linear actuators are best suited to operate in short cycles, as the motor easily overheat when running continuously. Electric linear actuators offer low maintenance and are available in a wide price range, corresponding with the production quality and feedback systems.

2.5 Mechanical Drives In Robotics

In robotics, electric motors suffer from their high speed and low torque characteristics, while the opposite is usually desired. Consequently, they need a drive system that converts the power to low speed and high torque. This could be achieved with a speed controller, but with substantially reduced efficiency [38]. The solution to the problem is to couple the motor to a drive with a gear ratio.

The linear actuator solutions presented in the previous section are already geared down. However, it is possible to adapt and change operation characteristics by designing converter mechanisms that utilize geometry and mechanics.

2.5.1 Timing Belts

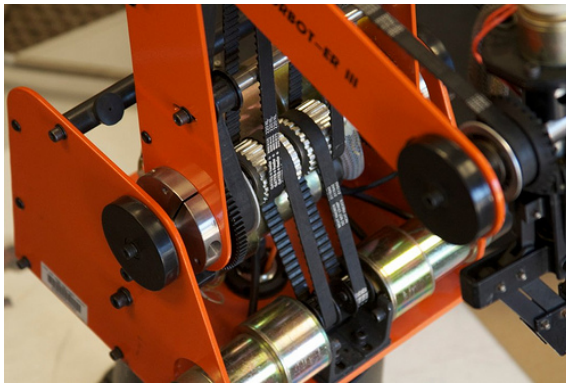
Belts for power transmission are available in different variations, notably; flat belts, V-belts, O-belts, and timing belts. The first three transfer power through friction forces on the smooth mating surface the pulley, thus the efficiency is relatively low and slip might occur. Timing belts, under correct tension, are synchronous as the belts have teeth and is driven around a sprocket, as shown in figure 2.4a. Synchronous operation is therefore convenient in robotic applications, as it ensures precise control over the position of the output shaft. Furthermore, timing belts can be used at high torque, very low rotational, speed and power levels up to 250 horsepower [38].

2.5.2 Bevel Gear

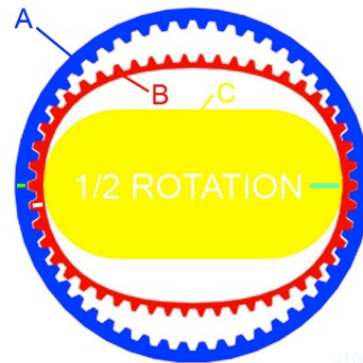
Bevel gears (figure 2.4c) are used in power transmission of intersecting shafts and is best known in the classic examples of differential drives and grain mills. Different types of bevel gears are characterized by teeth design, where torque and load capacity is mainly determined by the teeth's contact area and gear ratio. Thus, spiral teathed bevel gears have a greater capacity than straight bevel gears, but lower efficiency due to increased friction. Normal bevel gears has a typical gear ratio ranging from 1:1 to 5:1 [39].

2.5.3 Worm Drive

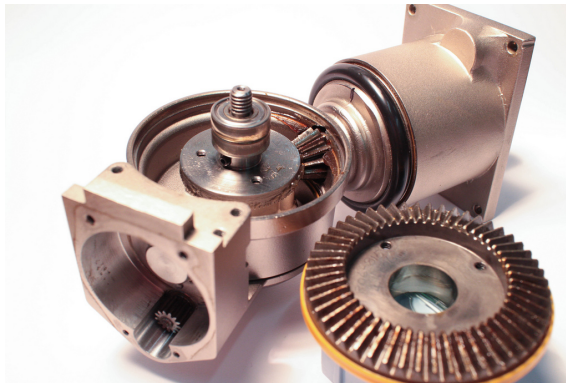
Worm drives (figure 2.4d) are built up by a screw/worm and a helical gear wheel, with typical gear ratios in a ranging from 5:1 to 300:1 [38]. The shallow angle of the teeth ensure that the wheel can not turn the shaft. As a result, worm drive is well suited for applications that require locking or braking capabilities.



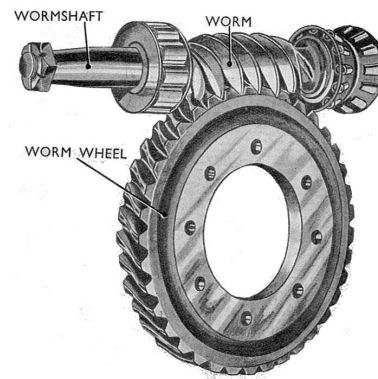
(a) Timing belt drives in a small robot arm, Society of Robots [40]



(b) Screen-shot from a harmonic drive animation, Lieshout [41]



(c) Bevel gears in a robot arm, Hudson [42]



(d) the principle of a worm drive, Government of the United Kingdom [43]

Figure 2.4: Four types of rotary actuators for robot arm joints.

2.5.4 Harmonic Drive

The harmonic drive speed reducer is used in high performance motion control applications, such as industrial robots, military and aerospace equipment. Harmonic drives are based on the principle of strain wave gearing, named after its primary torque transferring element, the flex spline (B in figure 2.4b). The figure also shows the rigid circular spline (A) and the ellipse shaped wave generator (C). As the flex spline is smaller than the circular spline, it must be deformed by the wave generator to engage the teeth with the circular spline. The number of teeth on the flex spline is usually two fewer than on the circular spline. By example, a gear ratio of 100:1 can be achieved with 200 and 202 teeth on the splines respectively [38].

In addition to the high performance speed reduction, the drive system benefits from the properties of precise positioning and zero backlash. The compact concentric shaft arrangement, torque capacities and efficiency makes this the number one gear design in robotics. However, harmonic drives are more expensive than traditional gear solutions.

2.5.5 Direct Drive

Direct drive mechanisms transfer the power directly from the motor without any gearing involved. In terms of robotics, gearing results in unwanted characteristics of backlash, flexibility, and friction. Which in turn complicates control [44]. There are many advantages in direct drives. Few moving parts reduce friction resulting in increased efficiency. This further extends the lifetime of the machine and reduce noise. Secondly, direct drive motors offers high torque at low rotational speeds with superior drive stiffness. Finally, the high torque and low inertia enables fast positioning and precise angular position sensing. Electric direct drive systems uses brushless DC motors, as they hold the desired torque speed characteristics.

Chapter 3

Materials and Mechanics

Chapter 3 focus on the use and properties of steel and aluminium, as they are the most common metals used in structural engineering of machines and vehicles.

3.1 Material Properties

The following definitions of material properties is found from Hibbeler's Mechanics of Materials [45].

Yield Strength [σ_y]

The yield strength is defined as the amount of stress a material can withstand before plastic deformation occurs. Below the yield point, the stress is in the linear elastic area, where the deformed material will return to its original shape once stress is relieved.

Ultimate Tensile Strength [σ_u]

The ultimate strength is defined as the maximum tensile stress a material can hold off before breaking. Consequently, it is used as a measure of the material's capacity to withstand elongating loads. Compressive and tensile strength capacities in metals are often closely related.

Modulus of Elasticity [E]

The elastic modulus, also known as Young's modulus, measures the stiffness of a solid material within the linear elastic area. It is defined by the constant relation between stress and strain. A low elastic modulus indicates a ductile material.

Shear Modulus [G]

The shear modulus, or modulus of rigidity, measures the materials capacity to resist shear forces. It is defined as the ratio of shear stress to shear strain.

3.2 Metal Alloys

An alloy is the product of a metal infused with other elements. Contrary to impure metals, the introduction of other elements is carefully controlled in order to achieve the desired physical properties. The main benefits of alloying are improved mechanical strength and corrosion resistance, but it can also reduce overall material cost. Alloys are in general divided into ferrous and non-ferrous categories. The materials can subsequently be divided into cast and wrought alloys, and further, treatable or non-treatable alloys.

Table 3.1: Mechanical and physical properties of aluminium alloys and structural steel. Table data from Rørvik [3]

Property	Aluminium Alloys	Structural Steel
Density	2.7 g/cm ³	7.9 g/cm ³
Elastic Modulus	70 000 MPa	210 000 MPa
Shear Modulus	26 000 MPa	80 000 MPa
Melting Point	650 °C	1530 °C

3.2.1 Steel

Steel represents the majority of ferrous alloys, with the exceptions of cast iron and some special iron-based alloys. Steel is extensively used in many industries due to the flexibility in strength, hardness, and the low production costs. However, steel is vulnerable to corrosion and has a relatively high density compared to aluminium alloys, as presented in table 3.1. Steel is easily welded and has a variety of production methods e.g. forging, casting, rolling, and pressing. Steel alloys are primarily composed of iron and carbon with additional elements of manganese, chromium, nickel and tungsten depending on the desired strength and corrosion resistance. As shown in the material data of table 3.2, the introduction of alloy elements increase overall strength. Meanwhile, the ductility is reduced and the material is therefore less impact resistant and more brittle at low temperatures.

In order to further improve the material properties, carbon steel can be hardened. The steel is heated up to 910 °C where the solubility of carbon is higher than at ambient temperature. The over-saturated solution of carbon is formed and locked by quenching the material. The many carbon atoms force the ferrite atoms to hold a martensite structure. The hardening process already improves the material strength at carbon-levels as low as 0.1% [46], although it is most common to harden steel with a carbon content greater than 0.8%.

3.2.2 Aluminium

Because of its poor strength, pure aluminium is not used in structural engineering. In order to obtain better mechanical properties, most aluminium products made from alloys. The strength can be further improved with strain-hardening or heat treatment. Although aluminium has lower shear and elastic modulus than steel, it is beneficial due to low weight, corrosion resistance, manufacturing speed and the possibility of fabrication through extrusion. On the other hand, the process of welding aluminium is intricate in comparison to steel.

Table 3.2: Composition and mechanical properties of a selection of steel alloys. Table date from Callister [4].

AISI/SAE or ASTM Number	Composition [%]	Yield Strength [MPa]	Tensile Strength [MPa]	Ductility [% El in 50 mm]
<i>Plain Low-Carbon Steels</i>				
1010	0.10 C, 0.45 Mn	180	325	28
A36	0.29 C, 1.0 Mn	220	400	23
<i>High-Strength, Low Alloy Steels</i>				
A440	0.28 C, 1.35 Mn	290	435	21
A656 Gr.1	0.18 C, 1.6 Mn	552	655	15

In structural engineering, the 3000, 5000, 6000, and 7000 series alloys are most common. The first digit of the association number is designed to the major alloy element.

Table 3.3: Composition and mechanical properties of a selection of aluminium alloys. Table date from Callister [4].

Aluminium Association Number	Composition [%]	Yield Strength [MPa]	Tensile Strength [MPa]	Ductility [% El in 50 mm]
<i>Wrought, Non heat treatable</i>				
1100-O	0.12 Cu	35	90	35-40
<i>Wrought, Heat treatable</i>				
5052-H32	2.5 Mg, 0.25 Cr	195	230	12-18
2024-T4	4.4 Cu, 1.5 Mg, 0.6 Mn	325	470	20
6061-T4	1.0 Mg, 0.6 Si, 0.3 Cu, 0.2 Cr	145	240	22-25
7075-T6	5.6 Zn, 2.5 Mg, 1.6 Cu, 0.23 Cr	505	570	11

The different heat treatments have a standardized designation system, marked by a letter, usually with one, two, or three digits assigned after the alloy's number. The most common are the letter O for basic annealing and the T temper codes. T temper codes are numbered from 1 to 10, each corresponding with a specific heat treatment process. For instance, T4 is solution heat treated and naturally aged into a stable condition in room temperature. T6 is also solution heat treated, but is artificially aged using a higher temperature. In general, high numbers represents high strength. A more comprehensive summary of the hardening designations can be found on MatWeb [47].

3.3 Structural Parts

3.3.1 Hot and Cold Rolled Steel Profiles

Structural steel profiles are fabricated in rolling mills, where the steel is rolled into its final shape. The process of rolling can be done while the metal is hot or cold. Hot rolling is

done by heating the steel to a temperature higher than the re-crystallization temperature [46] where the steel transforms easily. Hot rolled products are generally large in size. As the steel cools, it shrinks, making hot rolled steel suited in applications that do not require precise tolerances. Consequently, typical hot rolled steel products are railroad tracks and beams for construction.

Cold rolled products are further processed hot rolled products. The steel is run through reduction mills at room temperature before annealing or temper rolling. These methods produce closer tolerances and different surface finishes. Cold rolled steel are generally harder than hot rolled steel due to the high carbon content. Typical, cold rolled products are used in applications that requires close tolerances, special surface finishes, and straightness. Because of the additional processing, cold rolled steel usually costs more than hot rolled steel.

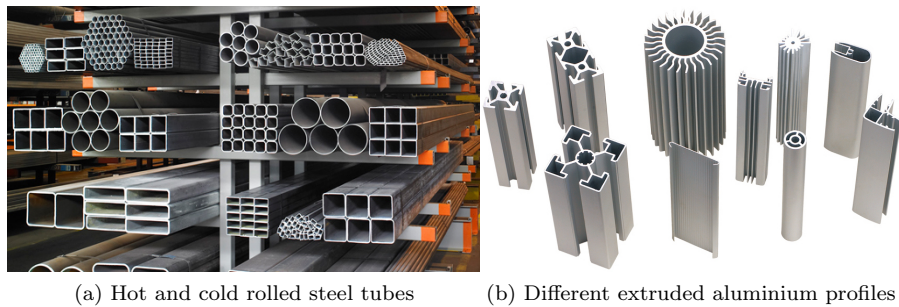


Figure 3.1: A variety of tubes and profiles available in steel and aluminium. Courtesy of Robor, PA International [14, 15]

3.3.2 Extruded Aluminium Profiles

Extrusion is a manufacturing method of great importance in the aluminium industry. It enables fabrication of profiles with cross-sections that would have been impossible to create with traditional manufacturing. Instead of relying on standard profiles, the engineer can easily design a cross-section for a specific purpose, considering fracture capacities, deflections, joints and special features. It is also possible to design hollow profiles.

The process of extrusion is done by heating aluminium bolts to a temperature of 400 to 500 °C in order to soften the material before it is pressed trough a die of the desired cross-section. Heat treatable alloys are often cooled directly as the material exits the die. Although most alloys of the 1000, 2000, 6000, and 7000 series can be extruded, the AlMgSi-alloys of hardening code T4 and T6 are most common [3].

3.4 Material Stress Properties

The following definitions of material stress properties is found from Hibbeler's Mechanics of Materials [45].

Tensile and Compressive Stress

Normal stress is defined as the intensity of the force action normal to the cross-section area. The normal stress is subsequently classified as tensile or compressive stress, if the force acts elongating or compressing on the element. Since F is normal to the area, A , then

$$\sigma = \lim_{\Delta A \rightarrow 0} \frac{\Delta F}{\Delta A} \quad (3.1)$$

Bending Stress

Whenever a beam is exerted to a normal force it will result in a linear variation in normal stress. The stress will vary from zero at the members neutral axis to a maximum value at the distance farthest away from the neutral axis. The bending stress is defined as the flexure formula

$$\sigma_b = \frac{My}{I} = \frac{M}{W} \quad (3.2)$$

Where:

σ_b = the maximum normal stress in the member, in the point on the cross-section farthest away from the neutral axis

M = the resultant internal moment, calculated about the neutral axis of the cross-section

y = the distance from the neutral axis to the point on the cross-section farthest away

I = the second area of moment of the beam

W = the section modulus

3.5 Joints

The term "joint" is in this thesis limited to two types of one-degree-of-freedom kinematic pairs; revolute (figure 3.2a) and prismatic (figure 3.2b) [48]. A revolute joint (also called pin joint or hinge joint) provides rotation around a single axis while a prismatic joint provides a linear sliding motion between two bodies. Prismatic joints can be shaped to resist rotation.

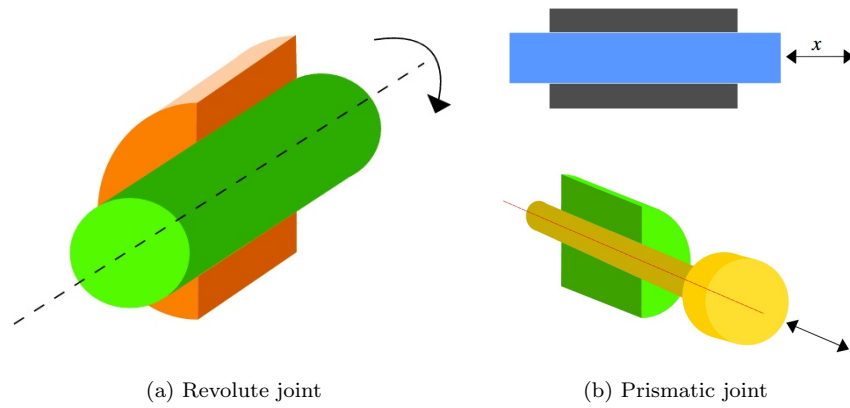


Figure 3.2: Principle sketch of two joint types. Courtesy of Wikimedia Commons [16, 17]

Chapter 4

Features and System Design

4.1 Conceptual Selection

The preliminary feasibility study of Bjurbeck [5] initially drafted three different implements for transportation of strawberry crates, presented in figure 4.1. The first sketch (a) shows a forklift implement, which enables Thorvald to handle pallets. Although it is suitable for some tasks in logistics, the concept poorly solves the challenge of handling individual crates in the field. The figure 4.1b illustrates a three link robotic arm mounted on the robot platform. The idea of a lightweight manipulator with range on all sides of the robot is, however, brought down by the difficulty of combining long range, high lifting capacity, and low weight. The third concept (c) is a simpler robot arm mechanism with two pairs of links and fewer degrees of freedom.

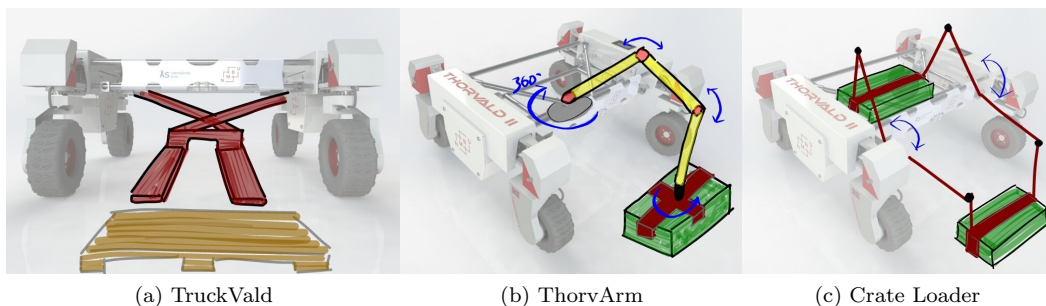


Figure 4.1: Sketches of the initial concept alternatives.

In order to evaluate the concepts and choose one for further development, each concept was evaluated based on a list of criteria and weighted on a tree-range scale. The selection matrix is presented in table 4.1 where the crate loader concept achieved the highest score and were chosen for further development.

The study proposed conceptual designs of one arm with one DOF and another arm with two DOF. Although the study at the time concluded that the design of the 1 DOF arm was successful, it was later found that the operation of the one DOF arm was not satisfactory. The arm could not move the end effector independently in the z -direction. The choice of

utilizing only one degree of freedom was taken to simplify the mechanical design and future control.

As the author started the work on this thesis, it was concluded that the system must have two degrees of freedom. The following sections describes the basic functions and design features of the two DOF arm, gripper head and base frame suggested in the preliminary study.

Table 4.1: Conceptual selection matrix of the feasibility study [5]

Criteria	TruckVald	ThorvArm	Crate Loader
Originality and innovation	1	3	2
Low complexity	3	1	2
Available market and low cost	2	1	3
Usefulness and interest	1	3	3
Low time of development	3	1	2
Academic relevance:	-	-	-
- Construction	2	3	3
- Design	1	3	2
- Personal progress	1	3	2
Easy to realise	3	1	2
Total score:	17	19	21

4.2 Basic Functions

The general idea is to design a mechanism with two parallel arms and a gripper head, as illustrated in figure 4.1c. In the field, the robot finds a crate and positions itself accordingly, while the arms sweep out over the crate. The gripper head is then lowered vertically until it envelops the crate before the crate is gripped by a pair of claws under the head. The arm will then sweep back and lift the crate up until it is finally released onto a bed within the robot's tubular frame. The robot can now move on to the next crate and repeat the process, or unload the crate to a given point. The operation sequence is illustrated in figure 4.2.

In order to enable the desired motions, the arm needs two degrees of freedom. The base link of the arm pivots around a revolute joint and, hence, serves an arc-motion. A variation in this motion changes both the x and z -coordinates of the base link's outer end joint. In order to allow more flexible motion patterns, a prismatic joint is introduced to the end link of the arm. The end link is constrained vertically by gravitation, thus the prismatic joint serves motion in the z -direction only.

As derived from the previous section, the mechanism only serves motion in the x and z -direction. However, to have a system that works in the field, the robot platform will contribute with its free motion along the x and y -axis, as well as rotation around the z -axis. This will allow the robot to pick up crates orientated parallel to the xy -plane. Nevertheless, the reality of the field environment is not that convenient. In a strawberry field, the plant rows hinder free movement in the y -direction and forces the robot to navigate on narrow paths in between rows. This also constrains the rotation of the robot, thus limiting the freedom of orientation of the crates. The problem could be solved by adding a revolute joint to rotate the gripper head around the z -axis, yet another degree of freedom would

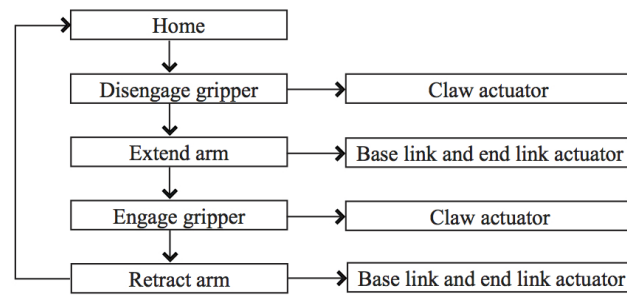


Figure 4.2: Flow diagram of the loader operation.

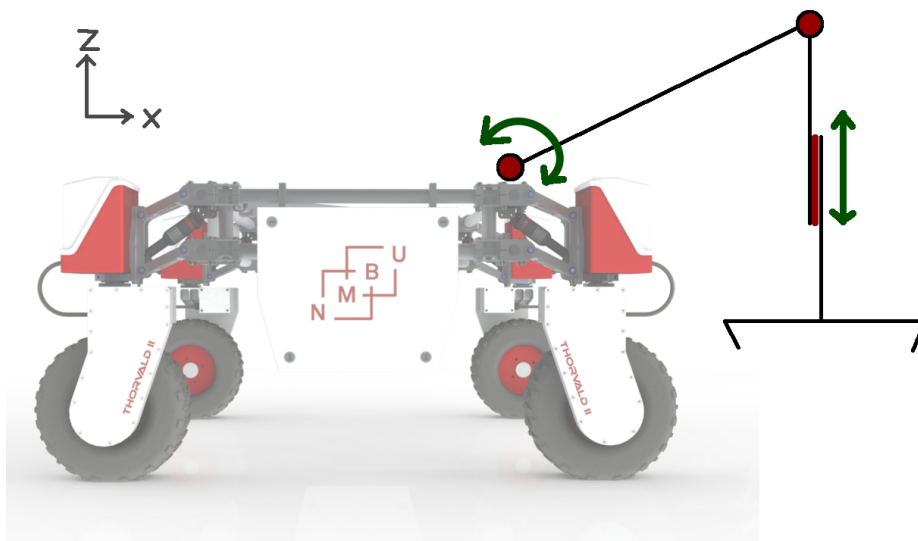


Figure 4.3: Illustration of the system's two degrees of freedom, with one revolute and one prismatic joint.

further complicate the design and control. Finally, the ground on which the crates lie are never completely level. This could be compensated for by introducing two more degrees of freedom with rotation around the x and y -axis to the head. These could be controlled with active joints or left passive if the gripper head is guided by e.g. sloped corner plates while the gripper approach and envelop the crate.

The crate bed inside the robot's frame should be able to hold multiple stacked crates. Also, the bed could have a system for handling several columns of crates, depending on the configuration of the robot.

As the robots are designed to be used in different applications, changing tools should be simple. Therefore, the crate loader unit should be able to hook up with the robot with minimal effort.

4.3 Design of the Arm

The design of the arm is built up by two pairs of parallel links, the base links and the end links respectively. The need for a set of parallel links is easily understood from the concept sketch in figure 4.1c, where the crate is lifted between the links and onto the robot platform. The arm links could be made from stock structural members, e.g. tubes or profiles. Their exact design depend on their desired features. Circular tubes are stiff in all directions, but complicate the joint design and mounting brackets etc. In comparison, using a rectangular tube makes mounting brackets and fabrication easier. Rectangular tube are also strong in their principal direction of the cross-section, but has less stiffness in the other direction.

In contrast to typical industrial robot arms, the joints of the crate loader could simply have a passive structural function. This certainly applies for the joint connecting the base link to the end link, as gravity is supposed to constrain the end link vertically. However, the joints should be tight enough to resist swinging of the end link.

A major concern in the design of the arm is how the forces of the actuator should be exerted and distributed. This will ultimately depend on the range and weight of the arm itself, as well as the desired lifting capacity. In the arm structure, the moment will sum up at the base joint. This is where the greatest material stress and shear forces will occur. The stress and forces needed to support and lift the arm can, however, be reduced by moving the point of attack away from the base joint. An example of this is shown in figure 4.4, where the point of attack is moved halfway up the arm and further displaced perpendicularly away from the arm's center line. This dramatically reduces the force needed to hold and lift the arm by utilizing basic beam theory.

In the case of the end link, the motion of the prismatic joint is linear and the counter force of the actuator is gravity. The end link actuator does not need to hold a moment relative to the arm length. The actuator simply needs to lift the crate, and will probably not need to reduce the working load through a transmission mechanism.

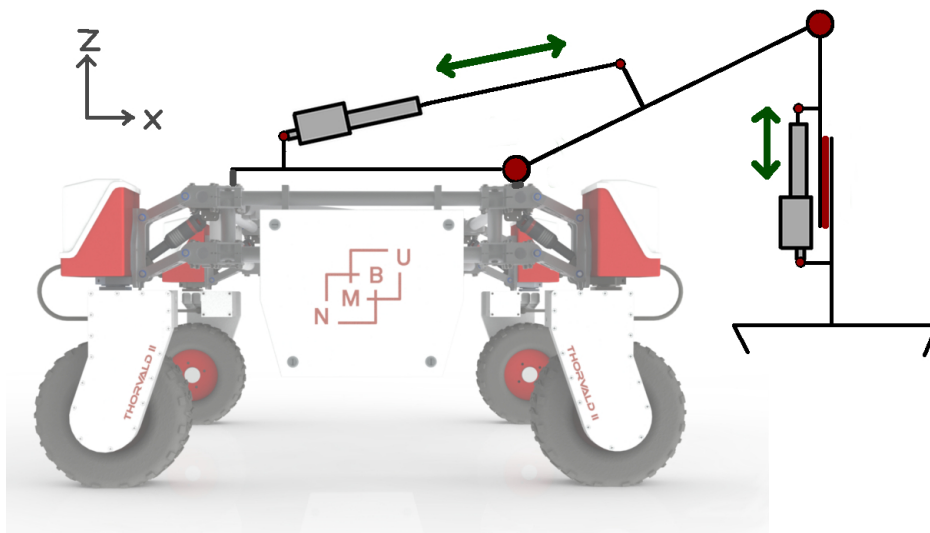


Figure 4.4: Sketch of a possible layout of the arm actuation.

4.4 Design of the Gripper

The gripper head design consists of a structural frame with a pair of claws that grip and hold the crate tight to the frame, while being lifted by the arm.

4.4.1 Gripper Frame

The gripper head frame is designed to lay down on top the IFCO-crate and envelop the outer edges. As the structural members of the frame envelop the edges, they will prevent the crate from sliding sideways within the gripper. In addition to supporting the weight of the crate, the frame should also be designed to reduce the needed precision for the robot to pick up the crate. This can be achieved by attaching a sloped skirt along the sides of the frame as seen in figure 4.5. When the gripper head is lowered down towards the crate, the sloped skirt will touch crate edges and subsequently push the crate and the gripper head to align with each other. The gripper head will continue to move until the crate is fully embedded under the frame. This procedure assumes that the gripper head is coupled to the end link of the arm with a passive joint.

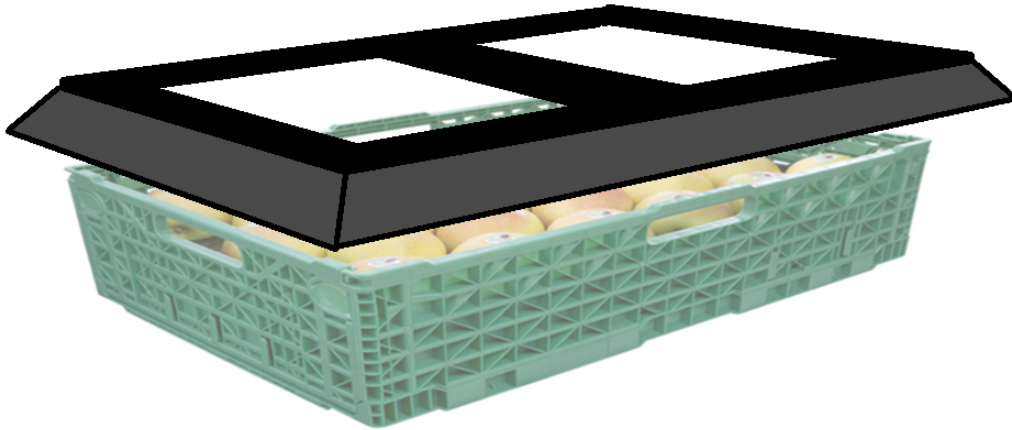


Figure 4.5: Concept sketch of the gripper head frame, with a sloped skirt providing self-alignment as the head envelops the crate.

4.4.2 Gripper Claws

The claws of the gripper are designed to replicate a human hand holding the crate by its handles. These claws can be designed to lift the crate and lightly press it up against the frame. Doing so reduces the risk of shaking that might damage the berries.

The claws could be actuated by a variety of motors with a double lever mechanism. However, the main criteria should be light weight and have low actuation speed. The need for sophisticated motor control is also limited, as the start and stop functions could be solved with simple end stop switches. An example of a possible mechanism design is illustrated in figure 4.6.

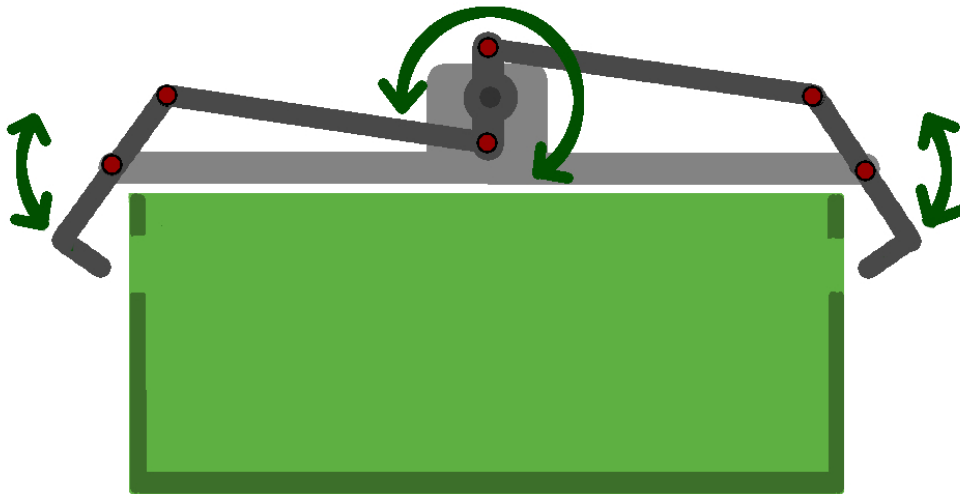


Figure 4.6: Sketch of a possible layout of the gripper claws.

4.5 Base Frame

The base frame of the crate loader is placed between the tubular frame of the robot platform. In figure 4.7, it is sketched on top of the tubes, reaching out in front of the robot. However, it could also be arranged in a different manner, e.g. rotated to extend over the robot's side or as a sliding rack that is easily hooked up with the robot. Ultimately, the arrangement will depend on the configuration of the robot platform and in what direction the loader will operate. This will be further assessed in chapter 6. A loading bed for the crates is also needed between the frame.

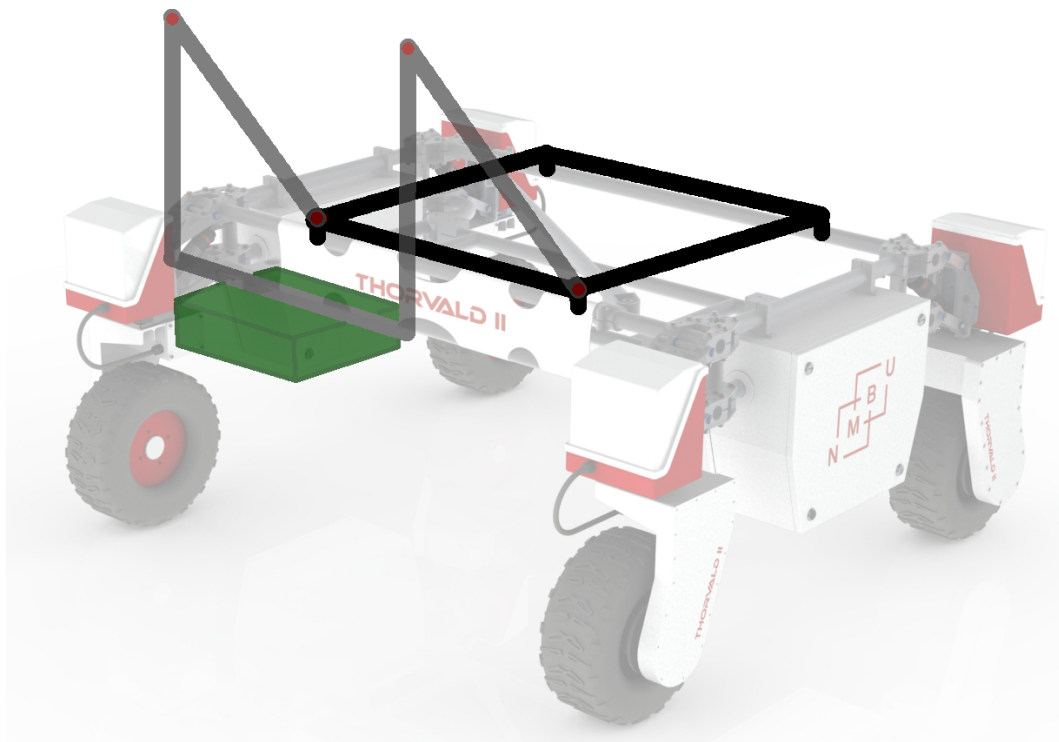


Figure 4.7: Simple sketch of the base frame principle.

4.6 Working Environment

According to Myhre, the strawberry production in Norway will most likely proceed in double rows (figure 4.8a) and on tabletops (figure 4.8b) in the foreseeable future. The loader implement is therefore designed to operate in both environments.

As the name implies, double rows has two rows of plants between each pair of tracks. Thus, they are the most space efficient plant pattern in use today. The row setup can be partly covered by large polytunnels as seen in figure 4.8a, or be out in open land, as seen in figure 1.2a. Between these rows, the robot platform has some room to maneuver sideways as well as room to slightly rotate without colliding with the plants. However, the only space for the pickers to leave the crates are the tracks, which require the loader to pick up crates directly in front of a wheel. Comparatively, the table-top rows allows the robot platform to operate between the rows, instead of over them, as seen in figure 4.8b. The implementation of the loader onto the platform will therefore be easier, as the loader has a less restricted workspace.



(a) Double rows inside a polytunnel



(b) Table-top rows inside a polytunnel

Figure 4.8: Row environments at Myhre Gård.

4.7 Metric Boundaries

The metric boundaries of the crate loader system are mainly driven by the size of the robot platform and the IFCO-crates. In order to provide a general overview, the basic dimensions are attributed and listed in figure 4.9 and table 4.2.

The table gives guidelines to the physical dimension of the crate loader, as a foundation in the final design process. All values listed in the table affects the capacity and range of the arm. The different row spacing influence the robot configuration and the final setup of the crate loader on the robot platform, which again influence the needed range of the arm. The height of the robot platform depends on the configuration of the robot. If the robot has no suspension it will be 74 cm, but adding suspension also adds an extra 10 cm to the height.

The IFCO-crates used in strawberry production are 60x40x18 cm, but has handles on all four sides (as shown in figure 4.5 and could therefore be loaded onto the robot in both directions. According to Myhre, these crates will most likely be used in the foreseeable future. However, the gripper should be easy to adapt according to different crate sizes.

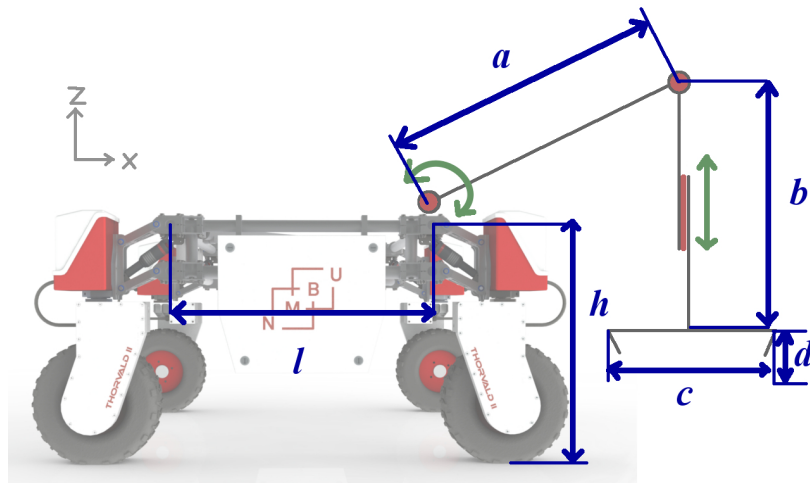


Figure 4.9: Metric boundary attributes.

Table 4.2: Metric boundaries of the crate loader system's attributes [cm].

	min.	ave.	max.
Base link (a)	60	80	100
End link (b)	50	70	90
Crate length/width (c)	40	-	60
Crate height (d)	-	18	-
Platform height (h)	74	79	84
Platform length (l)	85	-	-
Crate weight [kg]	7	9	11
Row spacing, open land double rows	-	160	-
Row spacing, table tops	-	135	-

Chapter 5

Component Selection

5.1 Actuation Components

The first step in the process of selecting actuation components is to determine the power source and whether to use rotary or linear actuators. The most important set of criteria for the actuator system are simple mechanical implementation and controllability. This implies that it is preferable to spend as little time as possible configuring a design of motors and drives. The ability to control the actuators is important in order in terms of implementing the control of the crate loader with the operating system of the robot platform. As the robot platform runs on electricity, it is natural to use the on-board electric system as the actuators power supply.

There are two alternatives in terms of actuation principles when using electric motors as the power source. The first option is to run pneumatic or hydraulic actuators with a central compressor or pump, powered by an electric motor. This allows variable drive of rotary and linear actuators. However, pneumatic and hydraulic systems have low efficiency and complicated design. Also, the process of automating and controlling such systems is too time consuming for this project and is therefore discarded.

This leaves us with the alternative of electric motors. As discussed in section 2.5, the high speed and low torque characteristics of most electric motors makes transmission drives necessary in order to supply the desired output speed and torque. The exception is direct drive motors, but the costs of such motors exceed the budget of the project. While the electric system of the robot platform has a voltage of 48 V DC, it would be ideal to find a motor with the same voltage. The voltage could be transformed to a lower voltage, which makes it possible to use 24 V or 12 V motors. Power transformation will be further discussed in section 9.1.

The short time perspective of the design process emphasis the need for actuators that are basically ready to be installed. Spending time finding matching parts and designing a complex system of motors and gears is therefore out of the question. This favors finding a system complete with a motor, gearbox, and a suitable feedback configuration. Furthermore, the implement is designed for use on an agricultural robot and needs to be dust- and weatherproof.

5.1.1 Actuation of the Arm

It is desirable to use the same motor type on both the revolute and the prismatic joint, in order to make the control of the arm easy. If a rotary actuator is to be used, it obviously needs a drive system that converts rotation into linear motion for the prismatic joint. A linear actuator must be able to supply rotational motion for the revolute joint. However, the rotation of the revolute joint is limited to less than 120° , suggesting that a linear actuator set-up as shown in figure 4.4 could work. The small angle of rotation certainly rules out the use of a direct drive mechanism. A critical factor of the actuator is the low rotational speed needed. If the lifting cycle is estimated to take 10 seconds to rotate 120° , the rotational speed of the output shaft will be around 2 rpm. As equation 5.2 show, the required torque is estimated to be around 100 Nm.

This makes gear types with a high gear ratio, such as worm drive or harmonic drive favourable. Finding a complete motor and gearbox unit with required low output speed and high enough torque proved to be difficult. Most motors with worm gears tend to have a higher output speed, while the prices of harmonic drives exceeds the budget of this project. Setting up a drive system with a timing belt, maybe in combination with gears, could allow the motor and gear to be located away from the joint. Further, a belt can transform rotational motion into linear motion. Using belts would require designing a purpose built drive system, and the idea is therefore discarded.

With the elimination of the rotary actuator alternative, the final option is to use electric linear actuators or linear motors. As one of the main set of criteria was simple implementation and control, the choice fell on using actuators. Linear electric actuators are available in a wide range of configurations in voltage, speeds, force capacities, and feedback systems. Ultimately, the quality of the feedback is the main factor in the evaluation of which actuators to use in order to control the system with the required precision. The feedback options are also what separate the cheap Asian made actuators from the more expensive ones produced in western countries.

5.1.2 Actuation of the Gripper

The challenge of finding an actuator for the gripper mechanism is somewhat similar to that of the arm. Here also, it is important to find a geared down motor unit that is easy to control. The demands for power and precision are, however, quite different. The actuator only needs to move the claws without any load. As the gripper lifts the crate, it needs to hold the position of the claws to prevent the crate from falling out. It is therefore favourable to use a worm drive, which has a good capacity of holding loads, as discussed in section 2.5. Motors with integrated worm drives are also widely found as stock items.

Another set of criteria is low weight and compact size, as it is desirable to keep the net lifting capacity of the arm as high as possible. The space available on the gripper head is also small, so there is little space for advanced mechanisms to actuate the claws. This eliminated the option of using a linear actuator or any drive option that require a certain amount of space, such as belt drives or harmonic drives.

In contrast to the arm actuators, the gripper does not require sophisticated control and feedback. The in/out position of the claws is the only feedback necessary. This can be provided by a pair of end stop switches.

After assessing different motor and gear options over the described criteria, the choice fell on using a brushed DC-motor with an integrated worm drive.

5.1.3 Linear Actuator - LinAk LA36



Figure 5.1: LinAk LA36 [6]

Table 5.1: Specifications of LinAk's LA36 [6].

Push/pull force, max.	2600 N
Self-locking force, min.	3400 N
Typical speed, full load	32 mm/s
Standard stroke length	100 - 999 mm
Motor	PM, brushed 24V DC
Typical current draw, full load	10.4 A
Weather and particle protection	IP66
Housing material	Casted aluminium
Spindle material	Stainless steel
Feedback signal	Absolute analogue 0-10 V
Weight with 350mm stroke	6 kg

After settling on the actuator type and consulting the local dealer, three equal LA36 (figure 5.1) actuators were ordered from LinAk in Drammen, Norway. The choice of model depend mostly on the force range, feedback possibility and IP-grade, while the specifications for each actuator hinge on several interdependent parameters. Firstly, the power available depends on the motor voltage, which also determines the current draw of the motor. Secondly, the integrated gearbox and spindle pitch co-relate to the push/pull and locking force, and the linear speed of the actuator. Thirdly, LinAk can provide different feedback options according to the type of controller the customer wish to use. Finally, the actuators of the LA36-series comes with the desired stroke length of the customer. The stroke length was determined in a practical geometric simulation done in SolidWorks, and was set to 350mm. The exact specs of the chosen LA36-model is found in table 5.1.



Figure 5.2: 24 V DC motor with worm drive.

Table 5.2: Specifications from the data sheet of the worm gear motor.

Motor	PM, brushed 24V DC
Rated motor power	3 W
Reduction ratio	350:1
Nominal speed, output shaft	24 rpm
Rated torque	1.9 Nm
Typical current draw, full load	10.4 A
Weather and particle protection	N/A
Feedback signal	N/A
Weight	150 g

5.1.4 Brushed 24 V DC-motor With Worm Drive

With the rise of global e-markets such as ebay and Alibaba, small electric components are now easily available and affordable. Although the items are easy to get, the product information and quality assurance is rather dubious. However, a cheap and simple worm geared motor (figure 5.2) was bought from a Chinese manufacturer.

The worm gear motor features self locking capacities, but the data sheet gives no further specification of the holding force. Also, there is no feedback from the motor, which require the claw mechanism to have end stop switches for control. The motor holds no promise of being weather-proof, and will eventually be replaced by a similar motor with a satisfactory IP-code.

Although the rated torque may seem low, the motor is assumed to be strong enough as the claw mechanism should be balanced in order to reduce the required torque.

5.2 Structural Components

As emphasised in section 5.1.2, it is essential to keep the net capacity of the arm as high as possible. The specific strength (strength-to-density ratio) of materials is therefore a major factor in the process of selecting materials for the structural parts of the design. Although this is most important in the design of the arm and gripper, and not so much in the base frame, it is also preferable to use the same material in the entire design. The two materials assessed (steel and aluminium) are widely available in stock structural profiles. The cost of aluminium profiles is generally higher than steel profiles. However, the cost of either material in the prototype build is considered a small post in the budget, so the choice of material is not economically motivated. As both materials offer good structural capacities, the choice is motivated by the specific strength of the material. Consequently, the general material of choice is aluminium.

The desired properties of the aluminium profiles is bending resistance in one direction and straight edges to enable the correct assemblies. Using circular tubes is therefore not an option, although they hold great bending resistance in all directions. Rectangular tubes, on the other hand, offer both straight edges and high bending resistance in the principal direction of the cross-section. The profiles size for the arms will be assessed in section 5.3.2. In order to simplify the assembly, the same size tubes will be used in both the base frame and the arm links.

Contrary to the structural members of the arms, the profiles used in the gripper head only need to hold a small load. The choice of profiles is consequently driven by finding a convenient size for the assembly and maintaining low weight. A straight angled profile in the dimensions 40x40x3 mm were therefore chosen due to its two perpendicular, flat surfaces with enough space for screw holes.

Extruded aluminium profiles are most commonly available in the 6000-series alloy with T4 or T6 tempering [3]. Both angle-profiles and rectangular tubes are available from the Norwegian metal supplier Astrup in 6060-T6 quality [49].

5.3 Design Verification

The capacities of the linear actuators and the structural members of the arm are verified in section 5.3.1 and 5.3.2. The final choice in profile shape and dimensions of the structural members is based on the calculation results. The required stroke length of the actuators and the links for the desired trajectory/workspace are found by trial and error in the CAD model. A workspace analysis will be presented in chapter 7.

5.3.1 Actuator Force

In order to assess the required capacity of the linear actuators, a calculation based on a static worst-case scenario has been set up. This means doing calculations with the maximum values from metric boundary values in table 4.2 to determine if the capacity of the chosen actuator is satisfactory. The actuator force needs to reverse the moment of the base link joint caused by the load at the link's end. The joint moment is a product of the link's end load and the length component perpendicular to the gravitational force. Thus, it is largest when the arm is extended horizontally. The length of the bracket (l_2) extending from the arm to the actuators point of attack is a major factor of the force needed by the actuator, as shown in equation 5.2. In this equation l_2 is set as low as 10 cm, but increasing it will further reduce the needed actuator force.

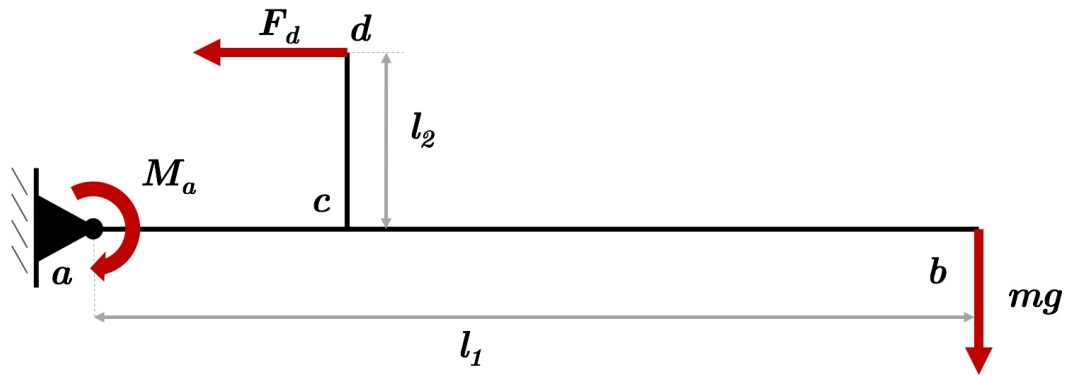


Figure 5.3: Free body diagram of a worst-case scenario of actuator load of the arm.

$$\Sigma M_a = 0 \quad (5.1)$$

From the free body diagram in figure 5.3, the moment in a is found:

$$\Sigma M_a = -mgl_1 + Fl_2$$

Where:

ΣM_a = the sum of moment around point a

$m = 10 \text{ kg} = \text{max. mass of crate (11 kg), one LA36 (6 kg), and estimated mass of the gripper head and arms (3 kg) divided by the number of actuators (2)}$

$g = \text{the acceleration of gravity}$

$l_1 = \text{length of base arm}$

$l_2 = \text{length of the bracket}$

$F_d = \text{pulling force of the actuator}$

$$F_d = \frac{mgl_1}{l_2} = \frac{10\text{kg} \cdot 9.81\text{m/s}^2 \cdot 1\text{m}}{l_2} = \frac{98.1\text{Nm}}{l_2} \quad (5.2)$$

$$F_d = \frac{98.1\text{Nm}}{0.10\text{m}} = 981\text{N}$$

Based on this result, it is safe to assume that the LA36 actuators with a pulling force of 2600N will be able to actuate the arm with the required loads.

5.3.2 Structural Capacities

In order to verify the capacity of the chosen material and arm link profile, the worst-case scenario of loads is continued with an assessment of material stress. This is done by finding the location and magnitude of the maximum stress, which include both bending and axial stress. The two are then combined in equation 5.3. The location and magnitude of the maximum stress is found in the moment diagram in figure 5.4iii. In the FBD (i), the force from the actuator bracket is converted to a moment and an axial force in the arm link. Furthermore, the shear diagram (ii) displays the shear force in arm link. The moment diagram is found by joining the integral of the shear diagram and the moment of the bracket force.

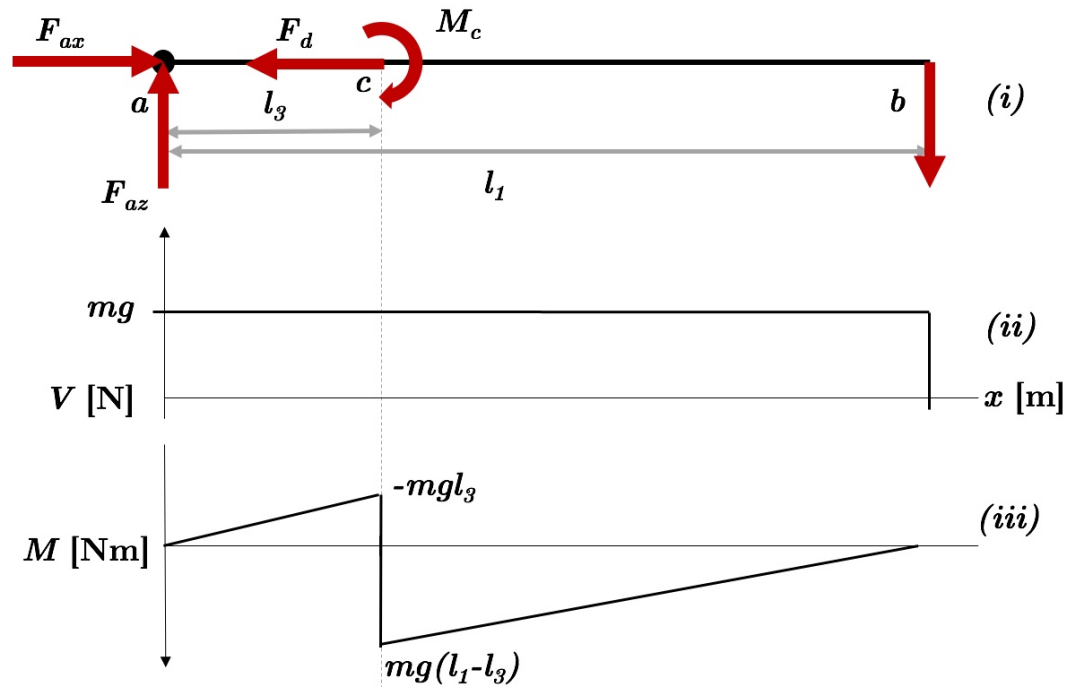


Figure 5.4: Free body diagram (i), shear (ii) and moment diagram (iii) of a worst-case scenario of structural loads on the arm.

Maximum total tensile stress:

$$\sigma_{tensile} = \frac{M_{max}}{W_z} + \frac{F_d}{A} \quad (5.3)$$

Where:

$$M_{max} = mg(l_1 - l_3)$$

W = section modulus of the arm link

A = the cross-section area of the arm link

As described in section 5.3.1, the moment from the actuator bracket, M_c , reacts to the moment from the end load. Therefore, the maximum bending moment is found at the

moment peak in point c . The value of l_3 is found to be 140mm from the geometric sketch block analysis.

In order to do the first assessment of the load case, a rectangular tube of 40x20x2 mm is found from the aluminum profiles catalogue of Astrup [49]. The cross section area and section modulus of the profile is respectively $224mm^2$ and $1877mm^3$. Then, using equation 5.3 the maximum tensile stress of the profile is:

$$\sigma_{tensile} = \frac{10kg \cdot 9.81m/s^2 \cdot (1000 - 140)mm}{1877mm^3} + \frac{981N}{224mm^2} = 49.3MPa$$

The total tensile stress is thereafter compared the material's yield strength to evaluate the stress capacity of the material. The capacity is expressed through the safety factor in equation 5.4:

$$n = \frac{\sigma_{yield}}{\sigma_{tensile}} = \frac{150MPa}{49.3MPa} = 3 \quad (5.4)$$

A safety factor of 3 indicates that only one third of the material strength is used in a worst-case scenario. Certainly, it is now safe to assume that using rectangular 6060-T6 aluminium profiles in the dimension of 40x20x2 mm will withstand the mechanical forces of the design.

Chapter 6

Assembly and Setups

Chapter 6 presents the final design of the arm and gripper head and the integration with the robot platform. The assembly was designed using SolidWorks 3D CAD software. The technical drawings and rendering were generated using the software.

Firstly, the different sub assemblies and parts are presented and followed by a brief explanation or comment. The modular concept of the robot platform and the possible configurations is then discussed before the choice of configuration is presented. The different setups of the implement mounted on the platform are finally presented with renderings, further explanations and two manipulated pictures of the complete unit in both working environments.

6.1 Gripper Head

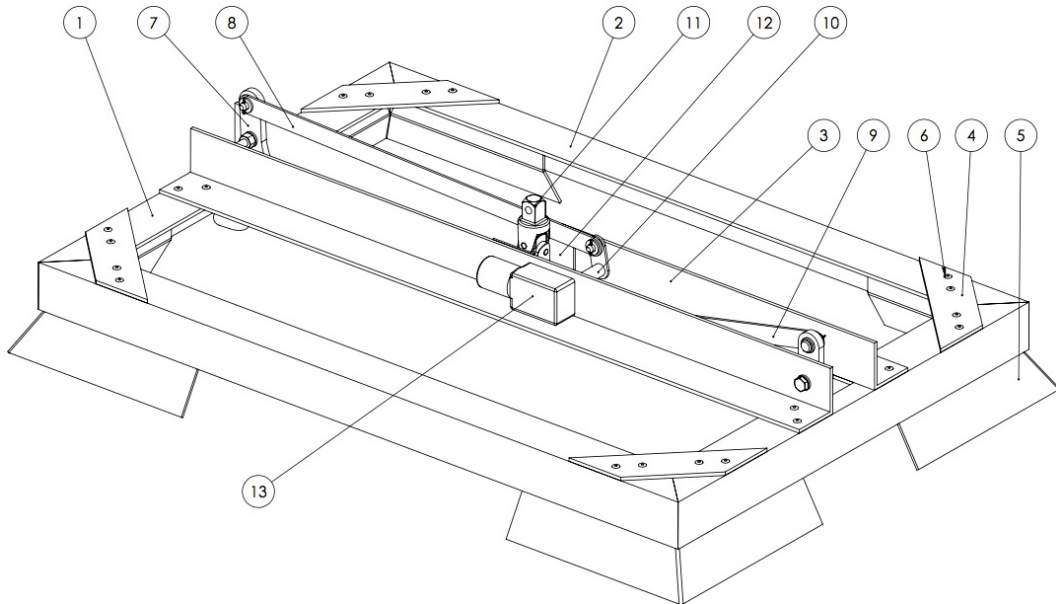
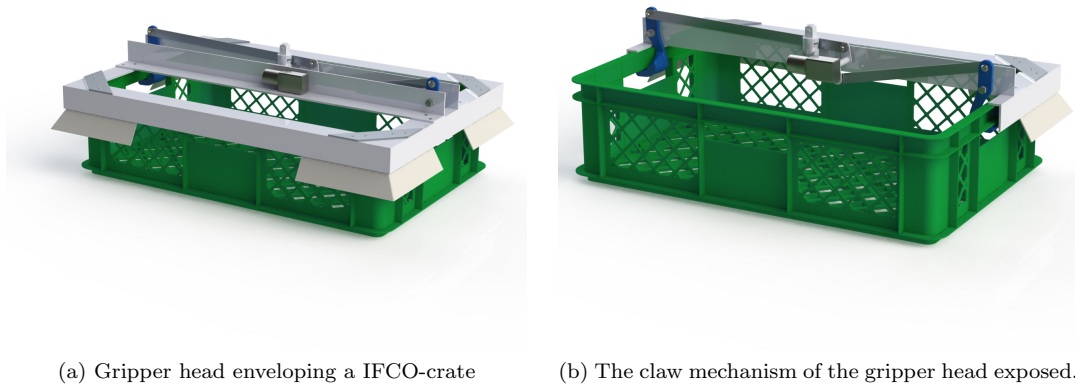


Figure 6.1: Part number call-out of the gripper head.

Table 6.1: Part list of figure 6.1.

#	Part
1	L-profile, 40x40x2, 420mm
2	L-profile, 40x40x2, 620mm
3	L-profile, 40x40x2, 620mm
4	Joint bar, 40x2, 150mm
5	Corner Skirt
6	Blind Rivet, 4mm
7	Claw
8	Claw link bar, long
9	Claw link bar, short
10	Adapter, axle-to-link bar
11	Universal Joint
12	Universal Joint Bracket
13	DC-motor with worm drive



(a) Gripper head enveloping a IFCO-crate

(b) The claw mechanism of the gripper head exposed.

Figure 6.2: The gripper head holding a strawberry crate.

The gripper head frame (figure 6.1) is assembled from four mitred L-profiles, four corner skirts, and a joint bar in each corner. These parts are riveted together, using 4mm blind rivets. On top of the frame, two L-profiles which adds stiffness and provide support for the claw mechanism and the universal joint are attached. The universal joint is the coupling of the gripper to the end link of the arm, and it allows some freedom of orientation for the gripper head around the x and y -axis, as required in section 4.4.1.

In order to allow the gripper head to easily envelop the crate, the inside measures of the frame is slightly bigger than the crate. Once enveloped, the crate is gripped and held tight to the inside of the frame by the claws. The claws are driven by double link mechanism, as shown in figure 6.2b, powered by the DC-motor with worm drive.

As the DC-motor and its axle-to-link adapter is mounted offset to the z -axis of the universal joint, the gripper head will be unbalanced once suspended from the joint. Therefore, the gripper head should be balanced by mounting a counterweight. The weight and position of the counterweight are easily found by practical trial and error once the gripper head is manufactured.

6.2 Arm Assembly

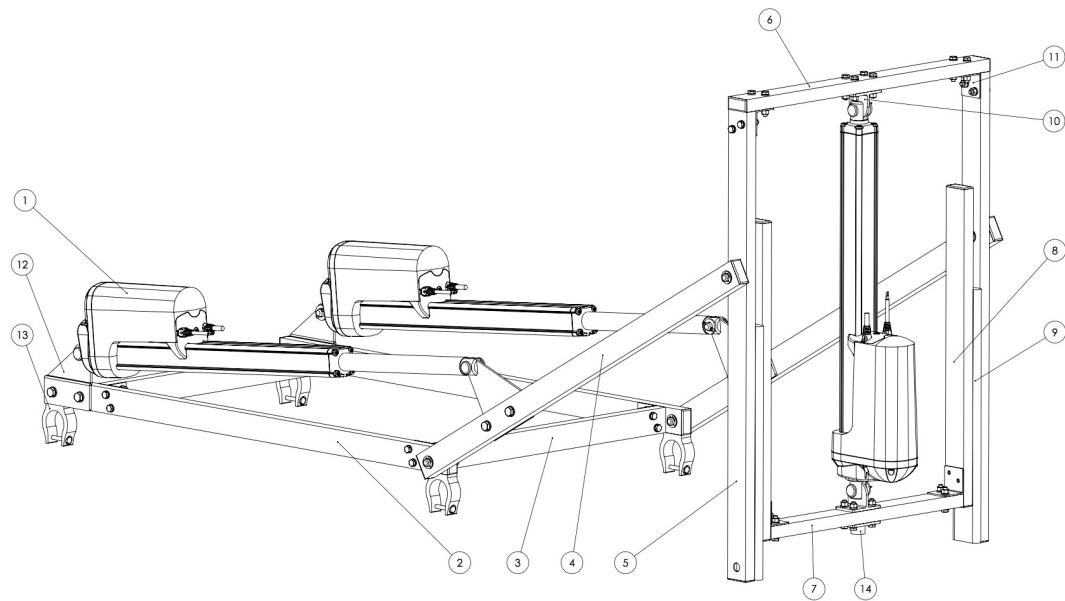


Figure 6.3: Part number call-out of the loader.

Table 6.2: Part list of figure 6.3

#	Part
1	Linear Actuator, LinAk LA36
2	Rect. tube, 40x20x2, 890mm
3	Rect. tube, 40x20x2, 490mm
4	Rect. tube, 40x20x2, 800mm
5	Rect. tube, 40x20x2, 740mm
6	Rect. tube, 40x20x2, 530mm
7	Rect. tube, 40x20x2, 420mm
8	Rect. tube, 40x20x2, 500mm
9	Slider
10	T-bracket for end link actuator
11	L-bracket for profile corner joints
12	Base link actuator bracket
13	Base frame-to-tube clamp, 40mm
14	Universal Joint Bracket

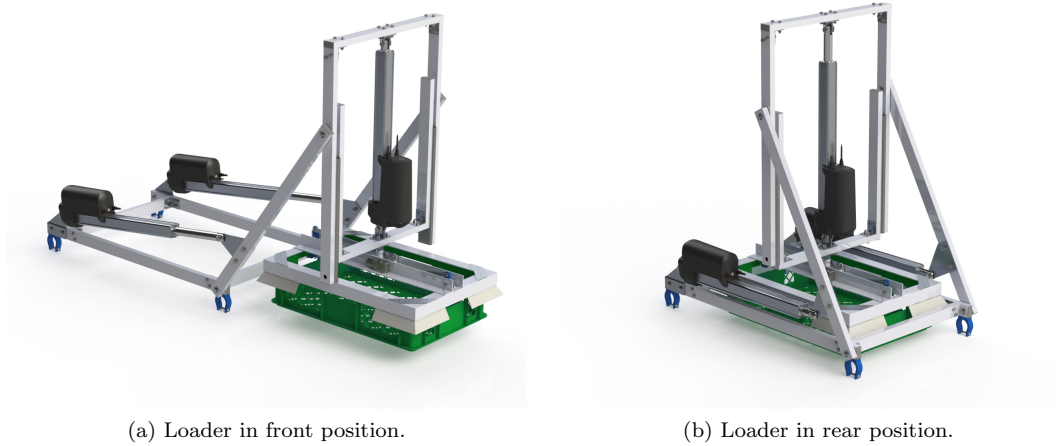


Figure 6.4: The complete assembly of the crate loader.

As shown in figure 6.3 and 6.4, the main structure of the design is built up by the rectangular tubes. The tubes are assembled to each other and the actuators with various brackets. Joint motion is served by the actuators, via the brackets and tubes. The base link joint revolves around pins, as shown in section 6.4.2. Contrarily, the prismatic end link joint runs along a slider to ensure smooth and guided motion. The exact slider design is not presented as there are numerous versions easily available on the market.

6.3 Base Frame and Crate Bed

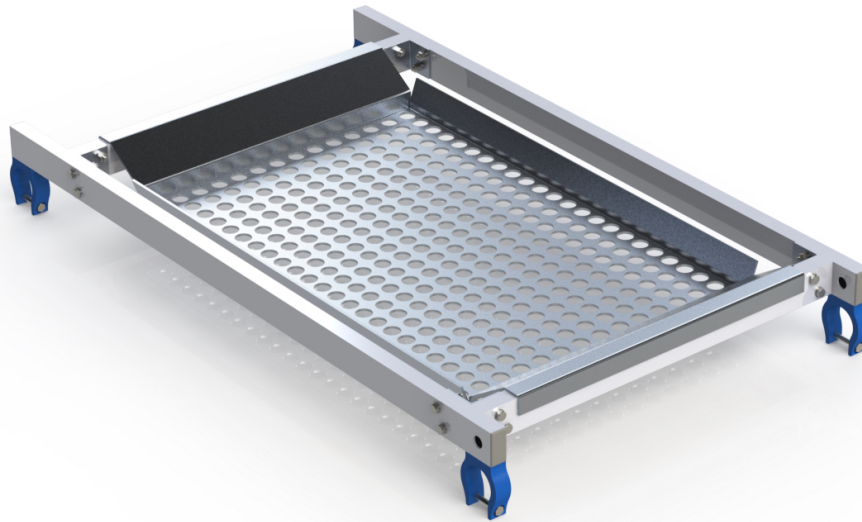
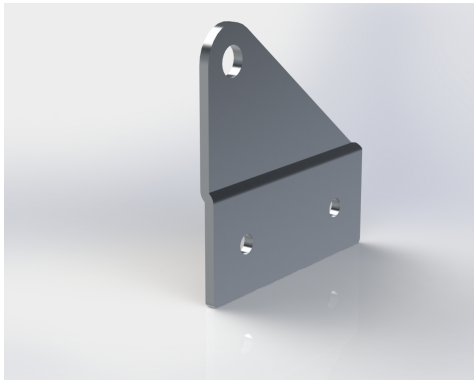


Figure 6.5: Base frame with the crate bed.

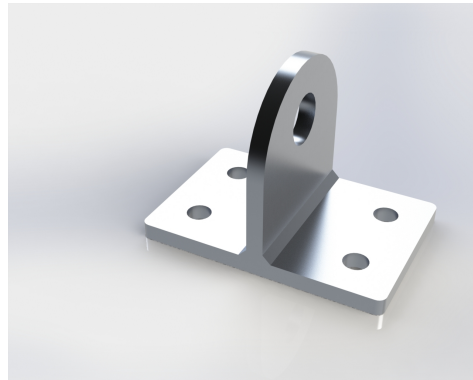
The structure of the base frame is similar to the rest of the loader, with rectangular tubes assembled with brackets. In the design of the crate bed, the base frame design is replicated and a bed plate is added between the tubes, as shown in figure 6.5. The bed plate is a simple 4 mm aluminium plate with buckled flanges on each short side. These flanges rest over the tubes of the frame, and is fastened with rivets or screws. On the long sides of the plate, a pair of slanted flanges guides and supports the crate into its final position. The plate base is perforated to reduce weight and allow drainage. Finally, the frame is mounted onto the robot platform using a set of four clamps on the lower side of the frame tubes.

6.4 Minor Parts of the Assembly

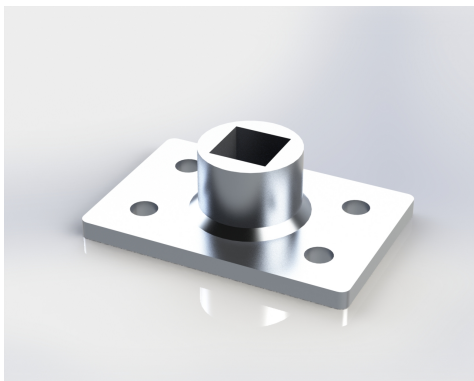
6.4.1 Brackets



(a) Base link actuator bracket.



(b) T-bracket for the end link actuator



(c) Universal Joint-to-end link bracket



(d) L-bracket for cornering tubes

Figure 6.6: Four brackets of the loader design.

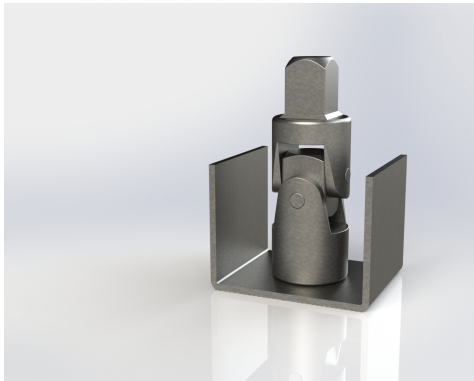
As shown in figure 6.3, the loader is made up of structural parts and components, which are mounted together with brackets. The rectangular tubes are assembled with a simple corner bracket (figure 6.6d), a standard part found in fastener catalogues or hardware stores. L-brackets provide decent stiffness and is the simplest way of joining two perpendicular members.

In the design of the loader, it was important to have sufficient space around the linear actuators and to elevate the point of attack in order to increase the moment induced by the actuator. This is realized by the bracket shown in figure 6.6a. From a slender 40x4 mm aluminium bar, the holes for the actuator mount and the tube attachment is drilled at their respective positions. Subsequently, the bracket is buckled twice to make the holes offset, to ensure alignment of each end of the actuator as they are mounted on offset tubes. The end link actuator is mounted in both ends with a standard catalogue T-bracket (figure 6.6b).

In order to attach the universal joint of the gripper assembly of the end link of the loader,

it was necessary to design a custom bracket. The bracket features a base with holes similar to the one of the T-bracket, but also a female connector to hold the universal joint's end. Joining the two parts can be done either by welding or by attaching a countersunk blind screw from the underside. The final decision should be made after assessing the materials available in the workshop.

6.4.2 Miscellaneous Parts



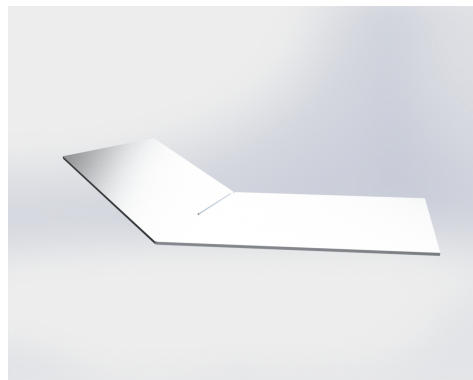
(a) The universal joint and bracket of the gripper.



(b) Claw in 3D-printed ABS-plastic.



(c) Motor axle-to-claw link adapter.



(d) Flattened sheet metal of the corner skirt

Figure 6.7: Miscellaneous parts of the gripper head.

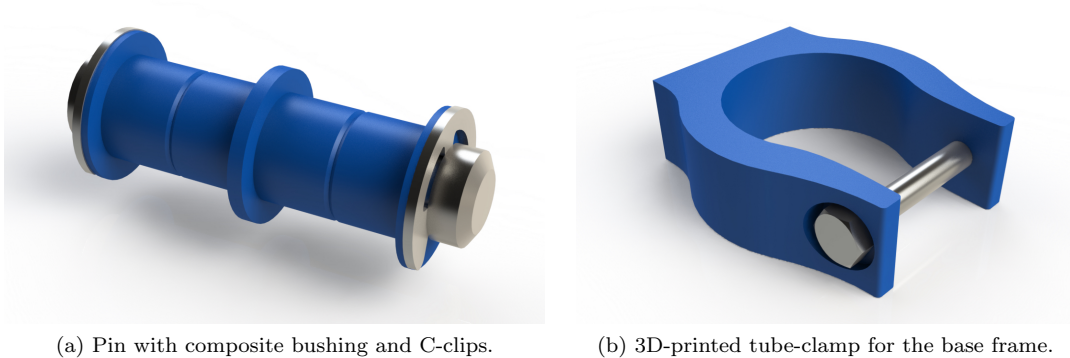
The gripper side of the universal joint is shown in figure 6.7a, with a U-bracket mounted on the female side of the universal joint. As the joint is made from tool-grade chrome steel, the bracket should be made from stainless steel to allow welding. The vertical ends of the bracket is fastened to the L-profiles of the gripper head with blind rivets.

The next rendering of figure 6.7 shows the design of the gripper claw. Imitating the fingers of a human, the lower end hooks itself around the handle of the crate. The claw pivots around the middle hole as the motor mechanism acts on the top hole. As the claw is

designed to be 3D-printed without a strength calculation, the first example should be tested to verify stress capacity.

Moving on, figure 6.7c shows the simple design of the adapter attached to the output axle of the DC-motor. The actuation force is exerted through a bar between the adapter and the claw.

Finally, figure 6.7d shows the flattened sheet metal of the corner skirts of the gripper head. From this sheet, the part is buckled, first by the corner and finally over the center-line of each end to form the flanges. The skirt is mounted to the L-profiles using blind rivets.



(a) Pin with composite bushing and C-clips.

(b) 3D-printed tube-clamp for the base frame.

Figure 6.8: Pair of parts of the loader design.

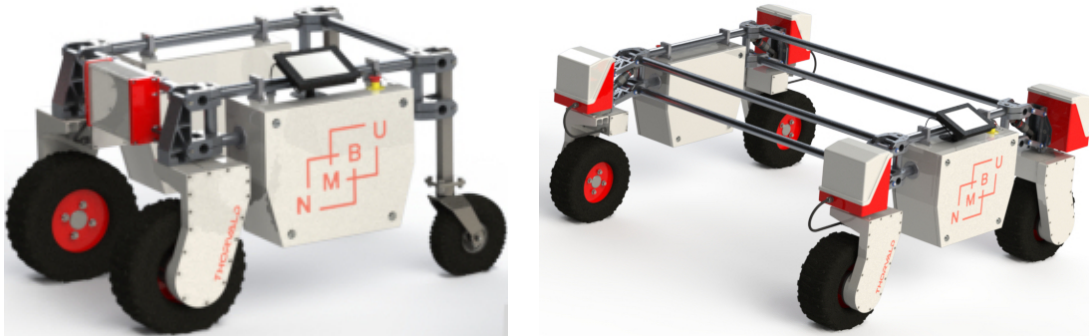
As described in section 6.2, the base link joint rotates around pins (figure 6.8a). To keep things simple, these pins are the same as some of the pins used in the robot platform. The pins are made from 12mm cold-rolled stainless steel, with a h7 ISO-tolerance. The pins are encircled by two pair of SKF composite bushings and retained by M12 C-clips. Using bushings between the holes of the base frame and the pins is essential to reduce friction and wear, and ensure a smooth motion.

In order to mount the base frame of the loader and crate bed to the tubular frame of the robot platform, the clamp shown in figure 6.8b was designed. As a suitable standard clamp could not be obtained, the choice fell on designing a 3D-printable clamp. Similarly to the gripper claw, this part should also be tested and verified to ensure that the holding force and the flexibility is sufficient. The claws are pressed perpendicularly down so it clips over the tube and tightens using a screw and nut.

6.5 Integration and Setups

6.5.1 Robot Platform Configurations

The modular design concept of the robot platform Thorvald II allows the robots to be assembled in a wide range of configurations and sizes. The cornerstone of the concept is literally the wheel module, which is divided into a steering module, and a propulsion module or passive wheel module. By combining the modules in different ways, each robot model can be tailored to meet the specific demands in propulsion and steering, according to the users wishes. Two examples of the configuration range are shown in figures 6.9.



(a) Thorvald II with differential drive and caster wheels

(b) Thorvald II with four-wheel drive and steering

Figure 6.9: Two examples of platform configurations.

Figure 6.9a shows a model with two propulsion modules in front and two passive caster rear wheels. The robot is steered by differentiating the rotation speed of the front wheels, while the rear wheels simply follow the track of the front wheels. This model exemplifies the most elementary, and least expensive, four-wheel robot configuration. However, the model has only two degrees of freedom (lengthwise and rotation around the z -axis) and low payload.

It is also possible to configure a stronger model with four propulsion modules. The steering is now controlled by differentiating the rotation speed of the wheels on each side of the robot, the so called skid-steer drive. The DOFs are the same as the differential drive model, but it has a higher payload. However, increasing the payload to a skid-steer robot contributes to increased damage of the top soil from tracking.

Figure 6.9 shows the use of wheel modules with both propulsion and steering modules, on a four-wheel steering and drive configuration. The complete wheel module enables the platform to utilize all DOFs of a robot designed to move in the horizontal plane (x and y -direction and rotation around the z -axis). Introducing the steering module to a four-wheel configuration also reduce the issue of tracking damage, allowing a higher payload than skid-steer configurations. The four-wheel drive and steering configuration can theoretically be expanded to a n -wheel configuration, as illustrated in the six-wheel robot in figure 1.1. Such configurations enable high payloads and could come to good use in farming logistics.

The wheel modules are mounted together using a clamped tubular frame, as shown in figure 6.9. The size or distance between the wheels, is determined by the length of the tubes.

Thus, it is easy to configure any robot into the desired size by adjusting the tube lengths accordingly. This applies for the tubes between the modules in both side- and lengthwise direction.

The enclosures on each side of the robot contain the batteries, electronics, and computer needed to operate the robot. Even though using two enclosures will provide space for a second battery package, it is possible to have a complete configuration with only one enclosure.

When operating over uneven ground, the configuration shown in figure 6.9 rely solely on the flexibility of the tubular frame. In conditions where the flexibility is not sufficient, it is possible to add a suspension module between the steering or propulsion module and the brackets on the corners of the frame, as shown in 6.9b. The suspension modules allows each wheel up to 20cm of vertical play relatively to the frame.

Choice of Platform Configuration

The choice of platform configuration is mainly motivated by the degrees of freedom. As the loader mechanism only operates in x and z -direction, the system depends upon the platform to serve motion in the y -direction and to rotate around the z -axis. This implies that the platform must have propulsion and steering modules on all wheels.

The working environment of the double-rows allows little space for the robot to rotate around the z -axis, while in the table-top environment, free space is limited. It is therefore practical to configure the platform with only two pairs of wheels. By evaluating these arguments, the four-wheel drive and steering configuration is chosen as the basic platform to carry the loader mechanism.

It is safe to assume that the robot will benefit from being equipped with suspension modules when operating in strawberry fields. When it operates between the table-tops, on the other hand, it can possible do without, as the ground is more level. Even though the setups presented in the following sections are without suspension modules, nothing stand in the way for future implementation.

6.5.2 Table-top Configuration

The main challenge of the table-top configuration was to make the robot platform fit between the support poles of the tables (figure 4.8b), while also having enough space to mount the loader and the crate bed between the battery enclosures. The total width of the robot platform in figure 6.10 is 106cm, while the actual distance between the edges of the support poles is 130 cm. Thus, there is some, but not much, space for the robot to maneuver sideways and rotate. As a consequence, the crates to be picked must be positioned on, and parallel to, the center-line between the rows.

As shown in figure 6.10 the workspace is unrestricted from nothing but the base frame, and the base links of the arm can pivot freely between the housing of the steering module.

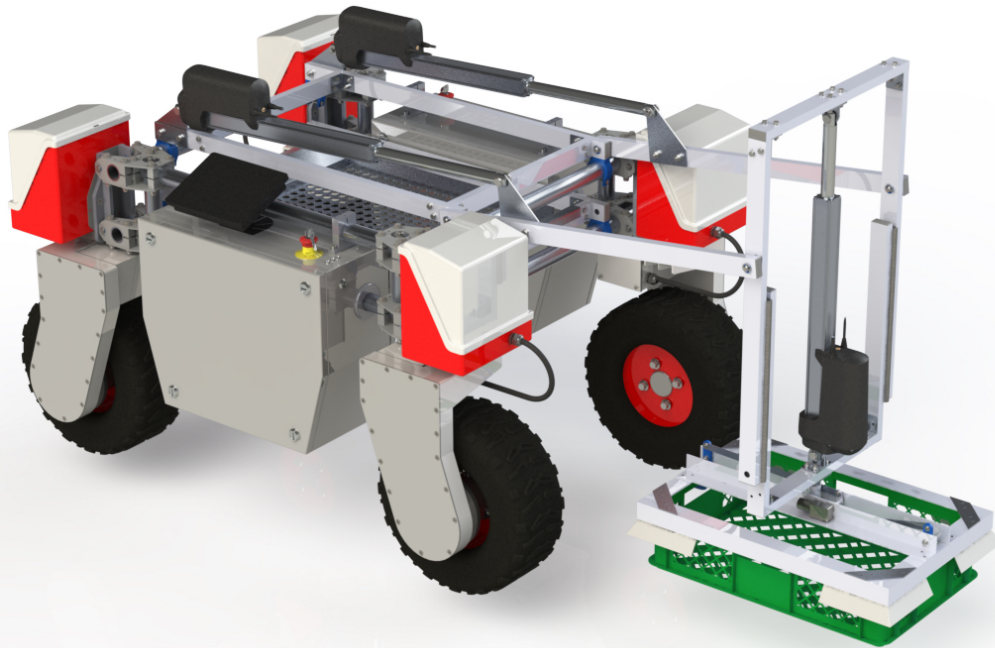


Figure 6.10: The loader implemented onto the most possible narrow platform configuration.



Figure 6.11: Rendering of the table-top configuration in it's right environment.

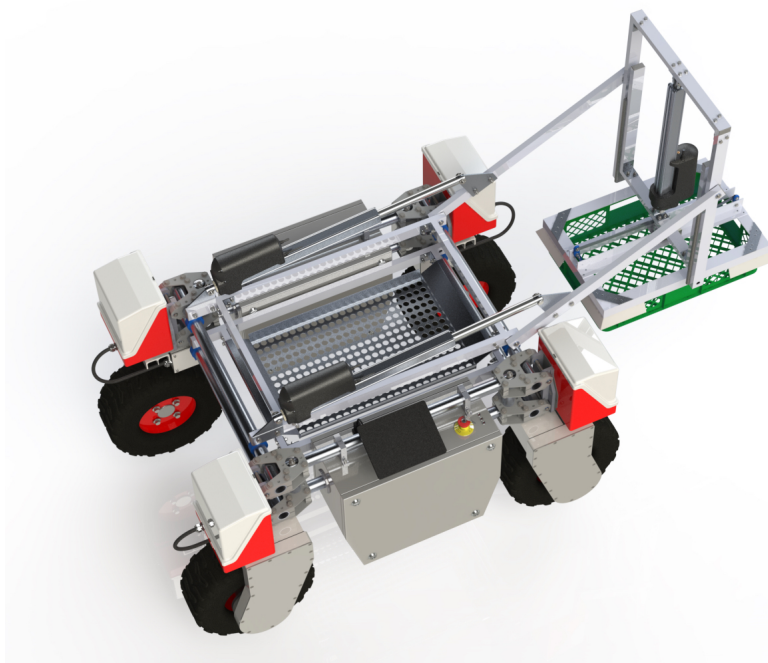


Figure 6.12: Bird's eye perspective of the loader in motion.

6.5.3 Wide Double-Row Configuration

The wide double-row configuration is an extended version of the table-top platform, made wide enough to span over three tracks. In that way, the middle track is free from wheels and the loader has the same unrestricted workspace as in the table-top configuration. The wide frame also have plenty of room for more sophisticated solutions for carrying multiple crates, which would make the robot more efficient. The frame of the wide double-row configuration has a free span of three meters. The setup shown in figure 6.13 will therefore most likely suffer from deflection and stiffness issues. The issues could, however, be solved by adding braces/stiffeners.

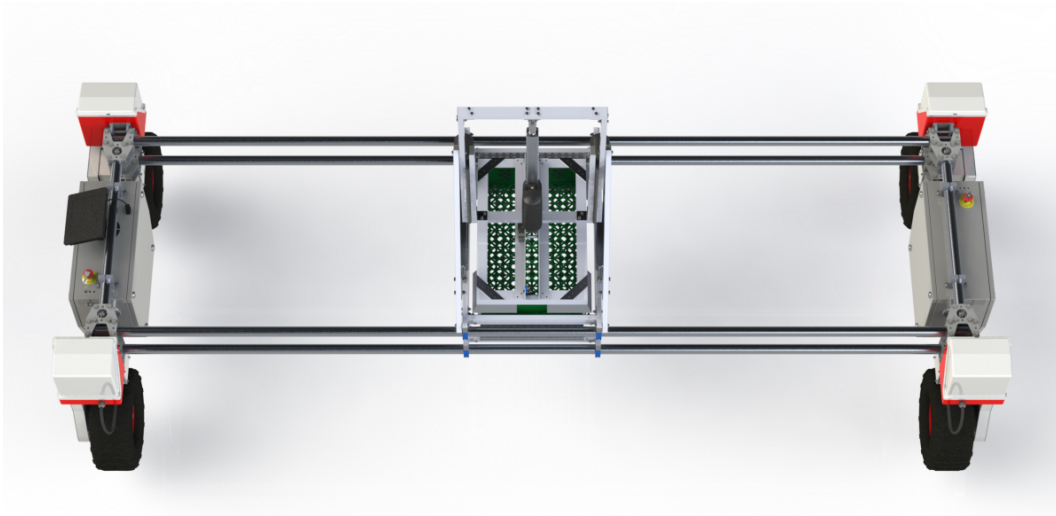


Figure 6.13: 3D rendering of the wide double-row configuration.



Figure 6.14: Photo manipulation of the robot platform in a double-row environment.

6.5.4 Narrow Double-Row Configuration

The narrow double-row configuration is an alternative to the wide configuration, and is designed to be able to move in two neighboring tracks. The arm extends over the steering module and in front of the wheel in order to grip the crate. To make space for the crate bed, one of the battery enclosures is removed. Thus, the battery capacity of this configuration is halved compared to the others. The housing of the front left steering module is removed to avoid collision with the crate, as shown in figure 6.15. Nonetheless, the issue can be solved by extending the length of the base links.

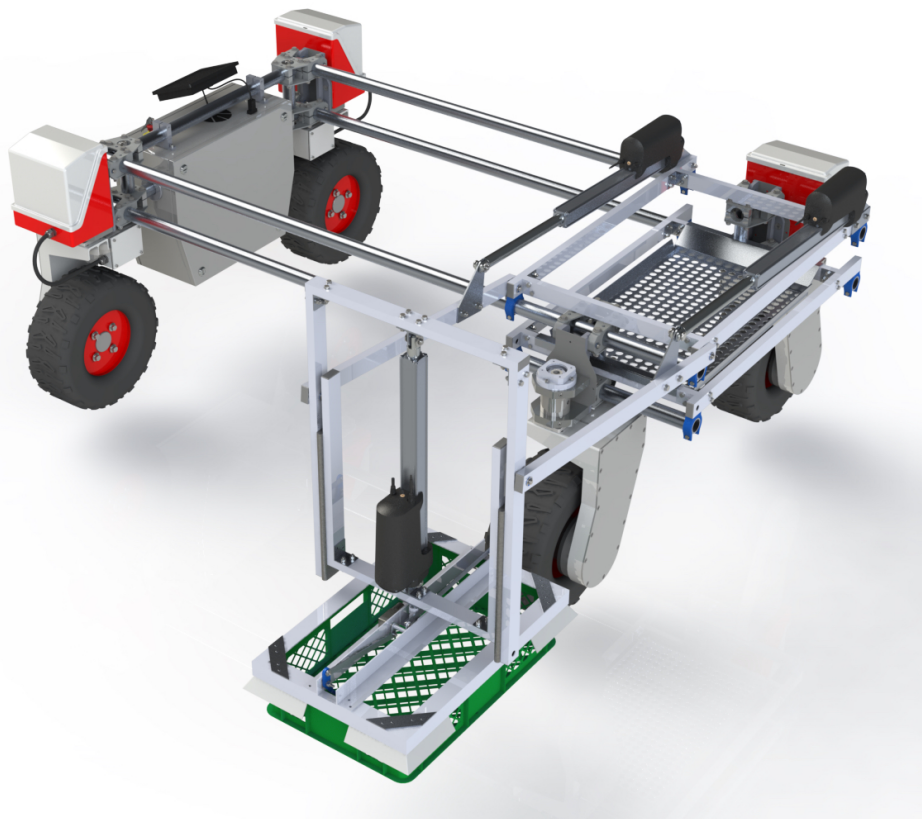


Figure 6.15: 3D rendering of the narrow double-row configuration.

Discussion Part I

Conventional manipulators are usually heavy with a high lifting capacity or lightweight with a low lifting capacity. Their high weight-to-capacity ratio is due to the need for precision, which means having mechanisms and actuators that are strong relative to their capacity. As Thorvald II is a lightweight mobile robot, it has neither the carrying capacity nor the power to sustain a strong conventional robot manipulator. The platform could however carry a conventional lightweight manipulator, but as implied above these lack the required lifting capacity. During the initial discussions concerning this project the first question was: *Is it possible to design a lightweight robot arm with sufficient range and the capacity of lifting a crate full of strawberries?* As the weight of industrial manipulators are consistent with their precision, the precision expected of such a lightweight arm is low. This led to the next question: *Are there ways to reduce the needed precision of the arm?*

The results of this thesis suggest that there are positive answers to both questions. Firstly, by designing a robot arm specifically for the task of lifting crates onto a mobile robot instead of making a multipurpose robot manipulator with needless precision and degrees of freedom. Secondly, by designing an end effector that has enough flexibility to self align with the position and orientation of the crate. And if the precision of the arm alone is not adequate, maybe the fidelity of the mobile robot's motion makes the precision of the vehicle-manipulator system sufficient. Although such a mechanism might not have the dexterity to justify being called a robot manipulator, it most certainly is a robot arm.

Process Evaluation

The preparations for the preliminary study started with the visit at the end user's (Myhre) farm to investigate the environment and discuss the needs of the end user. The end user was brought in to the process at an early stage in order to set up some of the critical parameters of the concept, as well as providing facts and data for the research. The importance of end user inclusion in the development process is emphasized in product development theories [50]. Whilst there was an early inclusion of the end user, the knowledge and competence of the subject could have been put to greater use. Especially considering that there was limited involvement, feedback and consultations regarding solutions after the thesis work had begun. A closer cooperation with the end user would probably have resulted in a design which would be closer to the likely end product.

A solid foundation in the initial phase of the design process is crucial in order to create quality products for the users, producers, and stakeholders. Before setting out to develop a new product, the actual needs and requirements must be carefully evaluated. The general requirements of the project was discussed the introduction of the thesis. However, the

technical design of the loader implement is just one part of a bigger project on utilizing mobile robots in agricultural logistics. While there have been a few discussions with farmer Myhre as well as within the robotics and control group, there is no coordinated overall plan for the project of using robots in strawberry harvest. In other words, the demands and possibilities of the whole project should have been properly mapped out and brainstormed. For example by analyzing how the robots should work logistically, fleet management, robot-human interaction and so on. Further, the process of conventional harvest involves many steps which may disappear with a future system. There is no point to developing technical solutions to a specific problem that might not be there if things were done differently in the end.

Despite the lack of an overall plan for the robotic logistics system, there is no doubt that the design and control of a crate loading implement to pick and transport IFCO crates still remains highly relevant.

Even though the feasibility study evaluated different options of actuation, a new and more comprehensive evaluation has been conducted in this thesis as study was not found thorough enough. Despite the meticulous assessment in part I, both assessments concluded that electric linear actuators should be used. A lot of time was spent re-evaluating the actuation types. In retrospect it is easy to say that this time rather could have been spent on the design process, but at the least the conclusion is made on solid ground.

The assessments of actuation and the structural members have been discussed qualitatively, and were initially set up in selection matrices (Pugh matrix) for a more quantitative evaluation. The approach was later discarded as the individual qualities of the various alternatives proved unsuitable for a quantitative assessment. Thus, a qualitative approach eliminating the unsuitable solutions was used.

Goal Attainment

The work of the thesis is concluded to have reached level 3 on the TRL scale. This was done by presenting analytic proof of the concept, in the form of capacity verification and component evaluation.

Design Evaluation

The overall quality of the design is difficult to evaluate and discuss before an actual prototype has been built. The loader mechanism is assembled from many structural members that are clamped and screwed together. It is therefore plausible that the sideways stiffness of the mechanism might not be adequate. The choice of using simple structural profiles was motivated by economical restrictions which constrained the use of complex manufacturing. Nonetheless, it is obvious that a more rigid design is possible if links were purposely designed instead of using standard profiles. Specially designed parts will also enable a simpler assembly with fewer parts.

The use of independent components such linear actuators, mounting brackets, and structural profiles eliminated the need to design distinctive links and complex joints. In addition to reducing manufacturing costs dramatically, assembling the robot arm from independent components enable the design to be easily reconfigured to change the workspace and lifting capacity of the arm. As the use of linear actuators and brackets eliminated the need of

complex joints with integrated actuators the combination of these and structural profiles are well suited for crane-like lifting mechanism.

The quality difference of the actuator components are radical to say the least. The requirements in control options are, however, very different. The linear actuators meets the requirement of being dust and rain proof, while the worm drive motor has no graded protection. Despite this fact, the choice of selecting the DC motor can be justified as the design is for a prototype only.

The design of minor parts in the assembly has not been determined by comprehensive assessments, but as simple and practical solutions that are easy to manufacture in a work shop. For the sake of building a prototype it is not important to have these designed deliberately, but can rather be refined at a later stage. It is also likely that there are suitable catalogue components available, although they were not found during the time span of the process conducting this thesis.

Gripper

The main point of concern regarding the success of the gripper design is the universal joint connecting it to the end link. As the gripper is designed to be passive, it is not unlikely that it could get out of balance. The design should be altered to include some kind of return spring mechanism in order to keep it horizontal but allowing it to align with the orientation of the crate.

Arm

The joint between the base link and the end link is designed to be passive. This means that the end link is hinged and constrained vertically by gravity. When the mechanism accelerates, the inertia of the link will most likely cause the it to swing from the passive joint. This complicate control and should therefore be fixed. The swinging could be reduced adding a radial torque damper or by redesigning the base link to a dual-link parallelogram design that would constrain the end link vertically and eliminate the possibilities of end link swinging.

Although workspace was considered during the CAD process, it would have been wise to include the workspace analysis at an earlier stage of the design process. The length of the links could then have been optimized according to the desired workspace. However, the modular design of tubes enables the links to be easily elongated or shortened.

Only one method was used to verifying the mechanical capacities of the arm's structural members. The common practice of mechanical engineering is to verify the design using CAD/FEA (finite element analysis) in addition to hand calculations. The choice of using one method only is justified by the fact that the design is meant as a prototype and that the loads are relatively low. Further, there is no threat to human safety if the mechanism should fail. Keeping the calculations simple was therefore considered sufficient, while saving precious time. However, using FEA to verify the design may be advisable before the product may enter commercial sales.

Integration with the Robot Platform

The main challenge regarding the design was to create an implement that could solve the same task in two distinctive environments. The qualities of the different setups have been

discussed in their associated sections. The table-top configuration and the narrow double-row configuration are evaluated as plausible solutions that are likely to work well. The success of the wide double-row configuration is however more doubtful. The crate loading robots will operate in environments with human workers. A robot occupying three tracks will probably conflict with their work.

Conclusion Part I

Part I of this thesis aimed to develop the mechanical design of a crate loader mechanism prototype for the robot platform Thorvald II. With the basis of a preliminary feasibility study of the project, the initial idea of the conceptual design was further developed.

Chapter 4 discussed the required mechanical features of the design before the final choice of solutions were discussed and presented in chapter 5 and 6. These chapters present the components and design of a robot arm operating in the xz -plane with two degrees of freedom. When mounted on the platform, the arm is free to operate in a 3-dimensional space, as the platform moves in x and y -direction, and rotates around the z -axis.

The robot arm has two pairs of parallel links made from rectangular aluminium tubes. The base links pivot around a revolute joint at the base frame, while the end link features a prismatic joint constrained by gravity in the z -direction. Each of the two parallel base links and the end link were actuated by LinAK LA36 electric linear actuators with a 350 mm stroke powered by 24 V DC motors. The use of linear actuators with mounting brackets eliminated the need to design complex joints, and is therefore suitable for simple crane-like mechanisms. It also allows the use of stock structural profiles as links. This eliminates the need to specifically design links and therefore reduce cost of manufacturing dramatically. The use of such links also enable the design to be easily reconfigured to change the workspace and lifting capacity of the arm.

The end effector of the arm is a gripper head with two claws, and the gripper head is hinged to the end link with a passive universal joint. The structural frame of the gripper is assembled from aluminium angles. Both claws are actuated synchronously by one worm drive 24V DC motor via a double link mechanism. The mechanism is design so that it is impossible for the crate to fall out when it is lifted.

The design of the entire assembly was enabled with parts requiring a minimum of manufacturing to be produced, while catalogue items and stock materials was pursued during the design process.

Chapter 6 presented the loader mechanism integrated onto three different robot platform configurations; one for operation in a table-top environment and two for a double-row environment.

Part I of the thesis brought the mechanical design up to level 3 on the TRL scale by analytically proofing the design capacities.

The presented configuration of the robot arm assembly is adequate for initial testing as a prototype for further development. However, the results of the testing may suggest altering the geometry of the design or changing the actuators. This is easy because of the modularity of the entire assembly.

Part II

Modeling and Control

Chapter 7

Mathematical Modeling

In order to control the loader based on position, the geometry of motion, or the kinematics, of the mechanism must first be assessed. Kinematics describes the motion of points and bodies regardless of their mass or the forces involved. The static kinematic analysis of the loader arm aim to describe the mapping from joint positions to the end effector's location.

Although the mechanism is modeled in a two-dimensional xz -plane, the analysis will be an important part of a future integration with the robot platform to form a vehicle-manipulator system operating in the three-dimensional xyz -space.

7.1 Kinematics

The goal of the kinematic assessment is to be able to express the position of the end effector (gripper) with respect to the positions of the joints and vice versa. Since the mechanism moves in a two-dimensional plane, the position vector of the gripper is defined as $P_{0e} = [x, z]^T$, while the joint vector of a two joint mechanism is defined as $q = [q_1, q_2]^T$.

The relation between P_{0e} and q is determined by the arm mechanism and is given by the *kinematic equation* [51]:

$$P_{0e} = f(q) \tag{7.1}$$

When the joint vector, q , is known, the calculation of P_{0e} is simple and the solution unique. The problem of finding the end position for a given q is called *forward kinematics*. When the motion of the mechanism is assigned to the robot the position or trajectory of the end effector is however given. Hence, the joint vector corresponding to the desired end effector position needs to be calculated. Accordingly, the solution is the inverse function of equation 7.1:

$$q = f_{P_{0e}}^{-1}(P_{0e}) \tag{7.2}$$

The approach of finding the required joint variables from a given end effector position is thus called *inverse kinematics*. Notably, the general solution of q may not be unique or exist at all, which usually makes the problem of the latter of the two equation more difficult to find.

7.1.1 System Geometry

The assessment starts with finding the interrelationship between the angle of the base link arm and the length of the associated actuator.

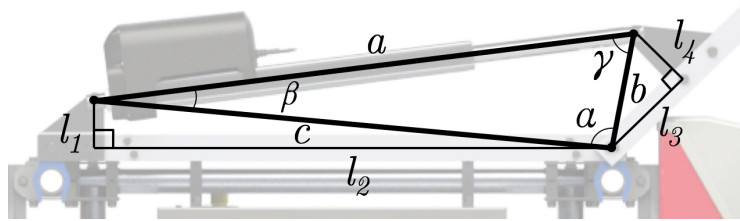


Figure 7.1: Cosine triangle of the base link actuator setup.

The triangle shown in figure 7.1 is first evaluated using the law of cosines:

$$a^2 = b^2 + c^2 - 2 \cdot b \cdot c \cos \alpha \quad (7.3)$$

Solving equation 7.3 for α returns:

$$\alpha = \cos^{-1} \left(\frac{b^2 + c^2 - a^2}{2 \cdot b \cdot c} \right)$$

The actuator is represented by a , while b and c are constants. Using the Pythagorean theorem, the length of b and c is calculated with the lengths specified in table 7.1.

Table 7.1: Length of lines in figure 7.1 and 7.2.

l_1	70 mm
l_2	784 mm
l_3	144 mm
l_4	100 mm
l_5	760 mm

$$b = \sqrt{l_1^2 + l_2^2} = \sqrt{70^2 + 784^2} = 787.12 \text{ mm} \quad (7.4)$$

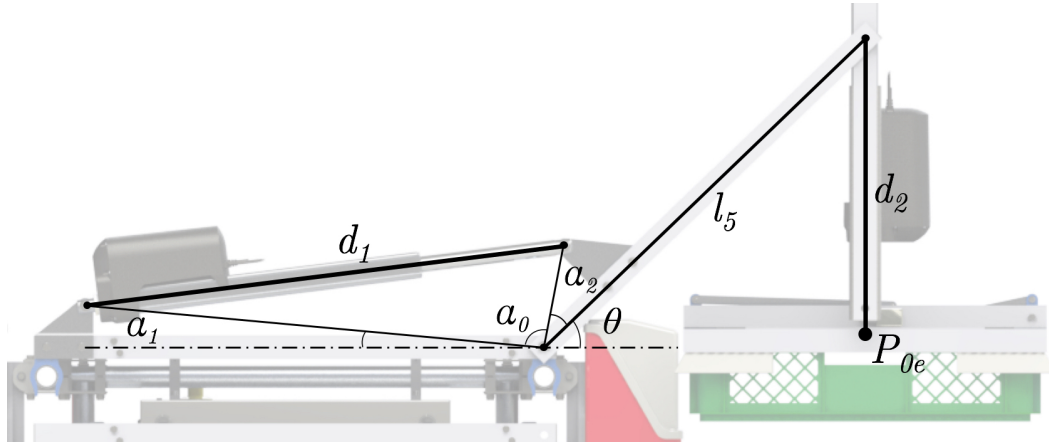
$$c = \sqrt{l_4^2 + l_3^2} = \sqrt{100^2 + 144^2} = 175.32 \text{ mm} \quad (7.5)$$

By inserting the numerical values of b and c , the angle α is expressed as:

$$\alpha = \cos^{-1} \left(\frac{175.32^2 + 787.12^2 - a^2}{2 \cdot 175.32 \cdot 787.12} \right) = \cos^{-1} \left(\frac{650295.00 - a^2}{275995.76} \right)$$

The angle of the base link, θ , is defined relatively to the horizontal plane xy and is a product of α_0 , α_1 , and α_2 , as illustrated in figure 7.2. The base link angle is then expressed as:

$$\theta = \pi - \alpha_0 - \alpha_1 - \alpha_2 \quad (7.6)$$

Figure 7.2: Joint variables of the actuators, d_1 and d_2 .

Thereafter, the angles of α_1 and α_2 are found:

$$\alpha_1 = \tan^{-1} \left(\frac{l_1}{l_2} \right) = \tan^{-1} \left(\frac{70}{787.12} \right) = 0.0887 \text{ rad}$$

$$\alpha_1 = \tan^{-1} \left(\frac{l_4}{l_3} \right) = \tan^{-1} \left(\frac{100}{144} \right) = 0.6070 \text{ rad}$$

When substituting α_0 , α_1 , and α_2 with their numeric values and the length a with the actual joint variable d_1 , the solution of θ is:

$$\theta = \pi - \cos^{-1} \left(\frac{650295.00 - d_1^2}{275995.76} \right) - 0.6957 \text{ [rad]} \quad (7.7)$$

Verification

Equation 7.7 is verified by calculating θ with the measured length of the base link actuator, d_1 , and subsequently comparing it to the measured base link angle θ from the SolidWorks model. From the 3D-model, the length and angle is found to be 864.54 mm and 29.51° .

$$\theta = \pi - \cos^{-1} \left(\frac{650295.00 - 864.54^2}{275995.76} \right) - 0.6957 = 0.51545 \text{ [rad]}$$

$$\theta = 0.51545 \text{ rad} \cdot \frac{180^\circ}{\pi} = 29.53^\circ$$

Comparing the result to the measured angle, it is safe to say that the mathematical expression of θ is precise enough to use in the control algorithm of the loader motion.

7.1.2 Forward Kinematics

The forward kinematics of the mechanism is found by obtaining the position of the end effector when the joint variables $q = [d_1, d_2]^T$ are given. First, the angle of the base link θ

if found from the joint variable d_1 using equation 7.7. The position of the end effector on each axis of the operational plane is then calculated using the equation pair 7.8. With the base link joint as the origin, the position of the end effector, P_{0e} , is found as:

$$P_{0e} = \begin{bmatrix} P_x \\ P_z \end{bmatrix} = \begin{bmatrix} l_5 \cos \theta \\ l_5 \sin \theta - d_2 \end{bmatrix} \quad (7.8)$$

7.1.3 Inverse Kinematics

As described in section 7.1, solving the inverse kinematic problem of the system is done by inverting the forward kinematic function. The geometry of the mechanism has only two degrees of freedom, where one joint serves motion in both x and z -direction while the second joint only moves in the z -direction. Finding the inverse kinematic equation is therefore simple, as it only has one solution. The forward kinematic equation is first solved for θ :

$$\theta = \cos^{-1} \left(\frac{P_x}{l_5} \right)$$

If θ was a direct joint variable, this would its inverse equation. However, the inverse kinematics control require the actual joint variables to be expressed as functions of the end position. θ must therefore be expressed directly in the as a function of the joint variable d_1 .

By going back to equation 7.3, d_1 can be expressed as function of α and the constants of the inner triangle of figure 7.1:

$$d_1^2 = b^2 + c^2 - 2 \cdot b \cdot c \cos \alpha$$

Solving equation 7.6 for α and substituting θ yields:

$$\alpha = \pi - \theta - 0.6957 = \pi - \cos^{-1} \left(\frac{P_x}{l_5} \right) - 0.6957$$

Combining the latter two equations and inserting the numerical values for b and c gives:

$$d_1^2 = 787.12^2 + 175.32^2 - 2 \cdot 787.12 \cdot 175.32 \cos \left(\pi - \left(\cos^{-1} \frac{P_x}{l_5} \right) - 0.6957 \right)$$

The square of the joint variable d_1 is now reduced to:

$$d_1^2 = 650295 - 275995.76 \left(\frac{P_x}{l_5} \right) \cos(\pi - 0.6957)$$

Moving on, the joint variable of the end link actuator is found by inverting the forward kinematic equation of P_z and substituting θ :

$$d_2 = l_5 \sin \left(\cos^{-1} \left(\frac{P_x}{l_5} \right) \right) - P_z$$

Finally, the joint variables are further reduced and the numerical value of the base link, l_5 , inserted. The inverse kinematic equations of the mechanism is found and the joint variables are now expressed as functions of the end effector's position:

$$d_1 = \sqrt{650295 + 278.76 P_x} \quad [mm] \quad (7.9)$$

$$d_2 = 760 \sin \left(\cos^{-1} \left(\frac{P_x}{760} \right) \right) - P_z \quad [mm] \quad (7.10)$$

7.2 Workspace

The workspace of the loader arm is defined as *the set of points that can be reached by its end effector* [52]. As the loader strictly operates in the xz -plane, the total workspace is the area swept out by the center point of the gripper when all joint positions are executed.

The work area of the arm is constrained by the geometry of the actuators and arm links, base frame members, crate bed, and the ground in addition to the operational range of the joint variables. The mechanical constraints of the joints found by measurements of the 3D model and are presented in table 7.2.

The workspace is illustrated in figure 7.3. Here, the end effector is defined as a point in the center of the gripper frame, coincident with the top plane of the crate. The upper and lower arcs represent the trajectory of the end effector with the end link joint fully retracted and extended respectively. The area between the black lines represents all possible positions of the end effector. However, the mechanical parts such as frame members, the crate bed, and the ground represent obstacles that must be avoided. The obstacles compose collision zones, marked in red.

Table 7.2: Limits of joint variables

Joint variable	Min. value	Max. value
d_1	620 mm	945 mm
θ (passive)	124.6°	-11.4°
d_2	460 mm	810 mm

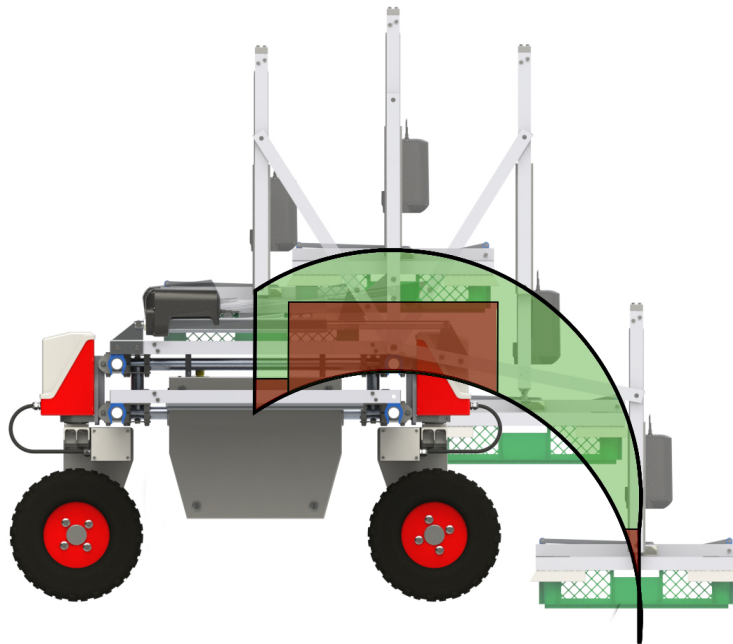


Figure 7.3: Workspace in green between the lines. Collision zones in red.

Chapter 8

Controlling the Loader

Controlling the motion and tasks of the robot platform and the loader require interaction between several different components. The orientation and position of the robot, actuators and links, and information concerning the robot's surrounding environment are all measured by sensors. Based on the sensor data, processors calculate the required actuation and command tasks according to the robot program algorithms.

Real-time control requires robust programs as well as reliable and efficient communication. It is therefore critical to choose the right methods and components in order to ensure a safe and predictable operation.

The following chapter covers the basics of process control, and the sensors and communication systems needed to design the control system and integrate it with the operating system of the robot platform.

8.1 Closed Loop Control System

A control system regulates the behaviour of a device or another system. An analogy to a control system is how the driver of a car constantly adjust the throttle in order to keep a constant speed in varying slopes. Comparing the speedometer to the desired speed, the throttle is increased or decreased accordingly. In robotics and automation, this regulation is done by a controller. A controller can be a standard computer, a standalone programmable controller, a PLC or PAC. A motion control system is set up by incorporating the controller with a motor, a drive or amplifier, and feedback sensors.

A closed loop motion control system (figure 8.1) continuously compare the status of the system with the desired input commands via feedback loops. Subtracting the feedback signal from the set point value generates an error signal which is used to correct the deviations from the input value [38]. Notably, controllers can regulate on signals of both speed and position. Closed loop systems are also called servo systems, as discussed in section 2.3.3. The motors of a servo-system has their own feedback sensors, typically encoders that measure speed or position. In some cases, the feedback sensors measure the load, or both the load and motor, as variations in velocity, position and torque often are caused by varying load conditions. In contrast, open loop systems run without any output measurement, and hence has no way of producing error-signals to regulate the output.

There are several types of controllers. The most common is the PID controller described in the following section. Other controllers may cancel non-linearities or try to predict

future behavior based on a dynamic system model. These model predictive controllers consider future time-slots by optimizing a cost function over a finite time range. For further descriptions of MPC and other controllers, see Gravdahl & From [53].

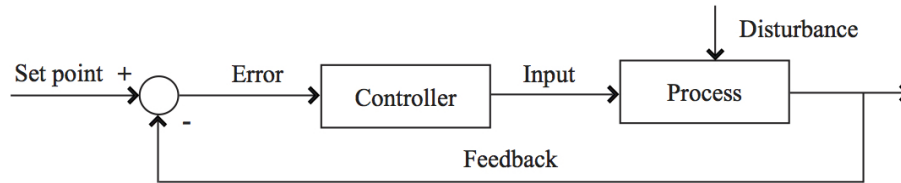


Figure 8.1: Block diagram of a basic closed-loop control system.

8.2 PID Controller

A *proportional-integral-derivative* controller continuously regulates on the basis of the error signal, and is a combination of the three control techniques of the name. The proportional controller's signal gain is directly proportional to the error signal, while the integral controller corrects the error accumulated over time. Further, the derivative controller's signal gain is proportional to the time derivative of the error, and thus compensates for sudden changes in the error signal. Each of these signals are finally weighted and summed up to control the process input. Even though it is the most used controller, the PID controller alone holds no guarantee for stability or optimal control. Most electric motor controllers uses some type of PID control.

8.3 Absolute Encoder

Optical absolute rotary encoders contain a set of photo detecting elements and light sources on each side of a code disk and a capture plate, as shown in figure 8.2. The photo elements generate pulses as the light is blocked at different sections of the code disk while the shaft rotates [18]. Contrarily to incremental encoders that only record changes in position, absolute encoders produce a unique signal for each distinct angle of the output shaft.

In some motion control systems, it is more suitable to use position feedback instead of speed feedback for control. Traditionally, speed control combined with a homing sequence (finding a reference position point) is used to control the motor or load position. However, it is possible to eliminate the need of homing routines and control directly on the position signal by using absolute encoders. Although the encoder itself does not detect change in position, it is possible to derive the position signal in order to find the speed. Hence, absolute encoders can also be used in motion control systems regulating on speed feedback.

Depending on the manufacturer, there are several techniques in transmission of absolute encoder signals, including analogue current or voltage, Ethernet Powerlink, Modbus or CANopen to name a few.

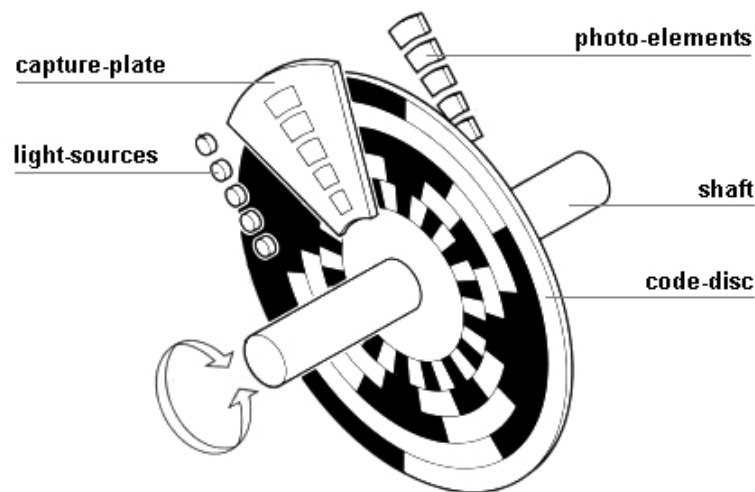


Figure 8.2: Basic principle of an absolute rotary encoder. Courtesy of Wiedemann [18]

8.4 Controller Area Network

The CAN bus (Controller Area Network) is a ISO-standardized method of serial communication, originally developed for the automotive industry by Robert Bosch GmbH in the late 1980s. Since then, it has evolved and is now often used in automation technology e.g. medical equipment, process industry and robotics. The major feature of the CAN is priority controlled message transmission through a twisted double wired cable and the use of a simple protocol with low computing power demand [30]. Further, CAN has a high immunity to electrical interference and outstanding abilities in repairing data errors and self diagnostics.

In traditional networks (Ethernet, USB), large blocks of data are sent from point to point, supervised by a bus master. CAN, on the other hand, broadcasts short messages to the entire network. Although a message is destined for a single or multiple nodes, all nodes of the network receive and acknowledge receiving the message. Thereafter, each node decides whether the message should be processed or discarded, based on the message ID. Hence, new nodes can be added to the network without reprogramming original nodes.

Since the designing process of the initial Thorvald prototype, CAN has been the communication network of all later models of the robot platform.

8.5 ROS: Robotic Operating System

Robotic Operating System is a set of frameworks for robot software development, providing the functionality of a operating system on a cluster of computers. The framework provides services involving message-passing between processes, hardware abstraction, device control, computing, package management etc.. ROS was originally developed in 2007 by Stanford Artificial Intelligence Laboratory, as a universal framework merging the fragmented work of the past on artificial intelligence sub fields.

The main ROS client libraries are written in Python or C++, and released under permissive open-source licences. Hence, a fundamental property of ROS is to support code

reuse, to allow researchers to truly develop new software instead of reinventing the wheel by writing the same codes as others. As of today, it is fully supported by Ubuntu Linux, while there are experimental versions of macOS and Microsoft Windows.

ROS is a distributed framework of processes called nodes. Control systems may consist of multiple nodes, each performing individual task like motion control, path planning, perception and so on. Consequently, it is possible to design executable programs or codes individually and have them coupled loosely at run-time. Nodes communicate *messages* by subscribing or publishing to *topics*. Each topic streams certain types of data, like images, control and actuation data and so forth. The topics may have multiple nodes subscribing or publishing, and each node may publish or subscribe to multiple topics. Thus, each node operates independently of other nodes. However, one-to-one communication is enabled using *services*, where a node can request a service and receive a response.

The ROS framework holds capable simulation and visualization tools. These tools enable developers to try out programs on computers before testing them in the real world, which reduce costs and improve safety. In the simulation environment, it is also possible to simulate the input of sensors, for example a camera, enabling a human to easily analyze sensor data. The representation of the robot model is enabled by using URDF files. Unified Robot Description Format is the standard XML representation of the robot model in ROS and defines the geometry, kinematics and dynamics of links and joints. Sensor simulation and collision avoidance can also be a part of the URDF-package.

Although low latency and reactivity is most important in robot control, ROS is not a real-time operating system. However, it is possible to integrate it to systems that transport ROS messages in and out of real time processes.

Today, ROS is implemented in robotic systems in anything from industry to hobby. It is also the framework of the Thorvald robot platform.

For further information on ROS, see ros.org [54].

Chapter 9

Architecture

Robot control involves processing and decision-making at different levels. The overall behavior is determined at a high level, while the low level processes control the different subsystems to operate according to the overall plan.

The following chapter addresses the control architecture of the loader mechanism implemented onto the robot platform. It also defines the components, the electric circuit and communication protocols. The system layout is shown in figure 9.1.

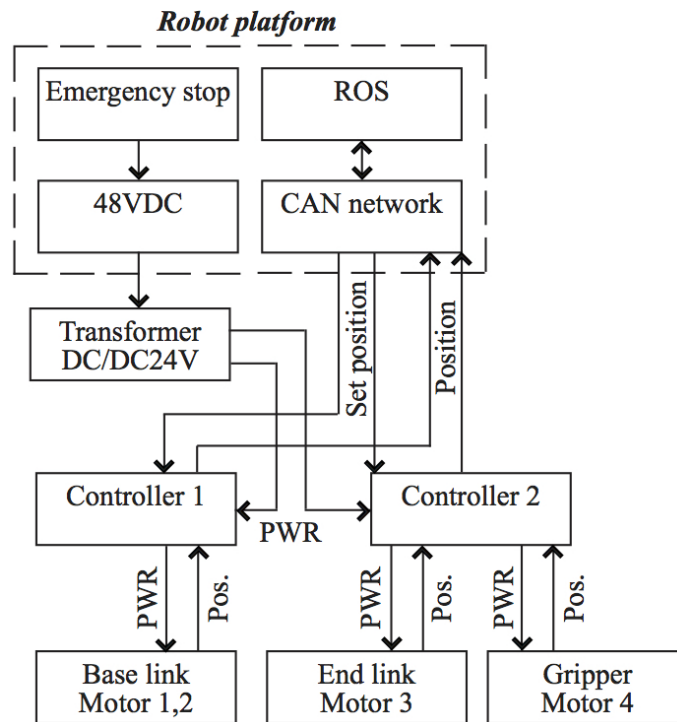


Figure 9.1: Architecture of the power and communication system.

9.1 Power Transformation

The robot platform's electric system has a nominal voltage of 48 Volts, while the linear actuators run on 24 Volts. Consequently, there is a need to transform the power in order to successfully integrate the loader mechanism onto the loader. Transformers, also called converters, come in a wide range of specs in terms of voltage intervals, power ratings, and transformation of current type (direct to alternating and vice versa).

The loader mechanism's peak power during operation occur when the base link actuators run at maximum load simultaneously. From the data sheet of the LA36, the rated current from each actuator at maximum load is 10.4 Amperes. The required power output of the transformer is found using Ohm's law [35]:

$$P = IV \quad (9.1)$$

Where P= power, I = current, and V = voltage.

The required power is:

$$P = 2 \cdot 10.4A \cdot 24V = 499W$$

With the established requirements, it was found that the electronics dealer Elfa Distrelec could deliver a suitable DC/DC transformer, shown in figure 9.2, within the budget. Although the margins of both power and output current are small, they are assumed to be adequate, as the calculations were done in a worst-case scenario.

Table 9.1: Specs of Mean Well DC/DC transformer [7].

Rated power	500 Watt
Input voltage	19 - 72 Volts
Output voltage	24 Volts
Max. output current	21 Ampere
Dimensions	215x115x50 mm



Figure 9.2: Mean Well 19-72V to 24V DC/DC converter. Courtesy of Elfa Distrelec [7]

9.2 Motor Controller - Roboteq SDC2160

The Roboteq SDC2160 is a generic motor controller, designed to run brushed DC motors. The controller features two independent channels of 20 A output at a maximum of 60V, and 6 digital or analogue inputs for commands or feedback. With its high performance microcomputer, it can perform advanced motion control algorithms in open and closed loops, speed and position modes. Also, the controller supports CANopen protocol and is easy to configure with the provided computer software. Furthermore, there are numerous safety features and options in the system architecture. The controller also support MicroBasic Scripting. This feature allows users to write programs that are permanently saved into the controllers Flash Memory. In that way, the capabilities of both a motor controller and a PLC or Single Board Computer is combined directly into the controller. The SDC-series are compact (73x73 mm) and weights 120 grams only.

As the Thorvald-project mainly uses and has good experience with Roboteq controllers, it was natural to choose Roboteq as the supplier without a comprehensive assessment of different controller brands and models.



Figure 9.3: Roboteq SDC2160. Courtesy of Roboteq [19]

9.3 Power Circuit

The four motors (three linear actuators and one DC motor) of the system is powered and controlled by two Roboteq controllers. Thus, the power circuit is divided in two circuit diagrams, although they share the same power source. The power source (the DC/DC transformer) has a maximal current capacity of 21A, which implies that only two of the actuators can operate together under full load. This must be considered in the control algorithm, unless the actual power consumption when operating all three actuators can be verified to be within the limits through tests. The claw motor will, on the other hand, operate when the actuators are at rest and has a negligible power consumption.

All signal connections will be soldered to a breakout board with a RS232 connector. This way it is easy to modify the connections during testing and to connect the controller

to a PC for calibration.

All three LA36s were delivered with a 0-10V feedback signal. However, the controller require the input signal to be within a range of 0 to 5V. Consequently, a voltage reduction-block of two resistors is added to each feedback signal cable, as seen in both figure 9.4 and 9.5.

The end stop switches of the claw motor break a +5V source current sent from the controller and return it to the one or the other analogue input. This will in turn be used in the control algorithm to determine whether the gripper is open or closed.

As the power circuit of the loader runs on 24V while the robot platform runs on 48V, it is absolutely necessary that the loader is electrically isolated from the platform. This is ensured by either isolating the earthed chassis of the loader, or run all earth wires back to the negative side of the power source.

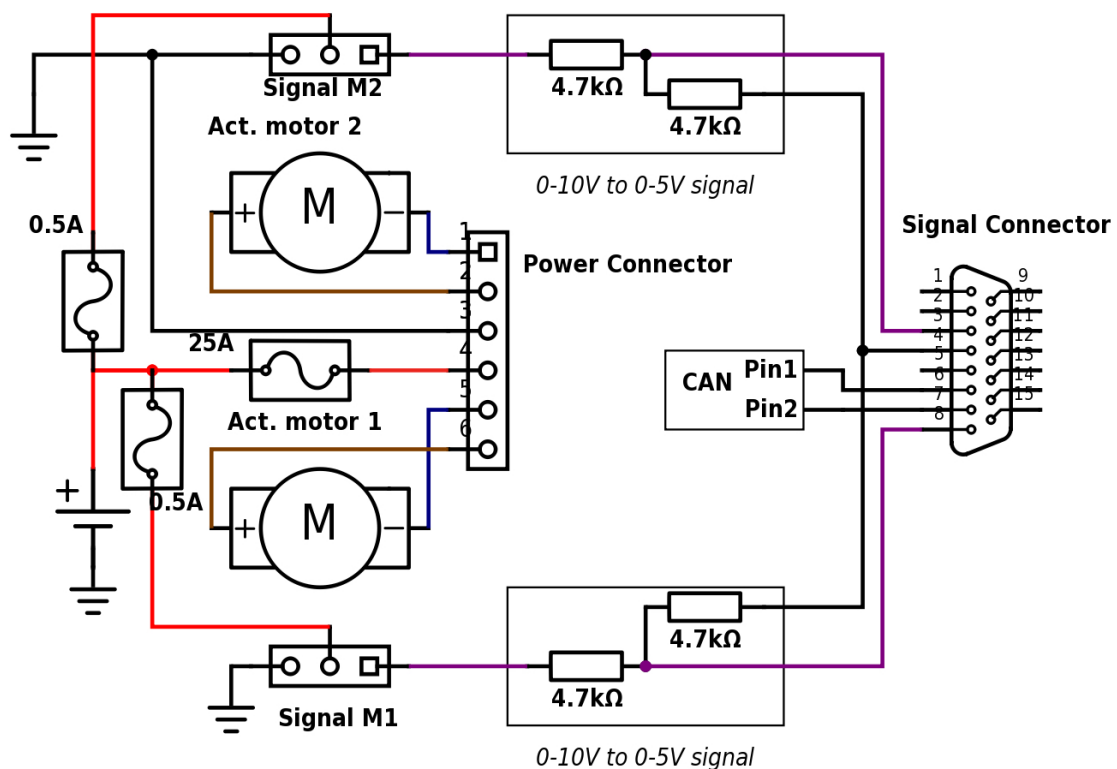


Figure 9.4: Circuit diagram of the parallel base arm link actuators and controller.

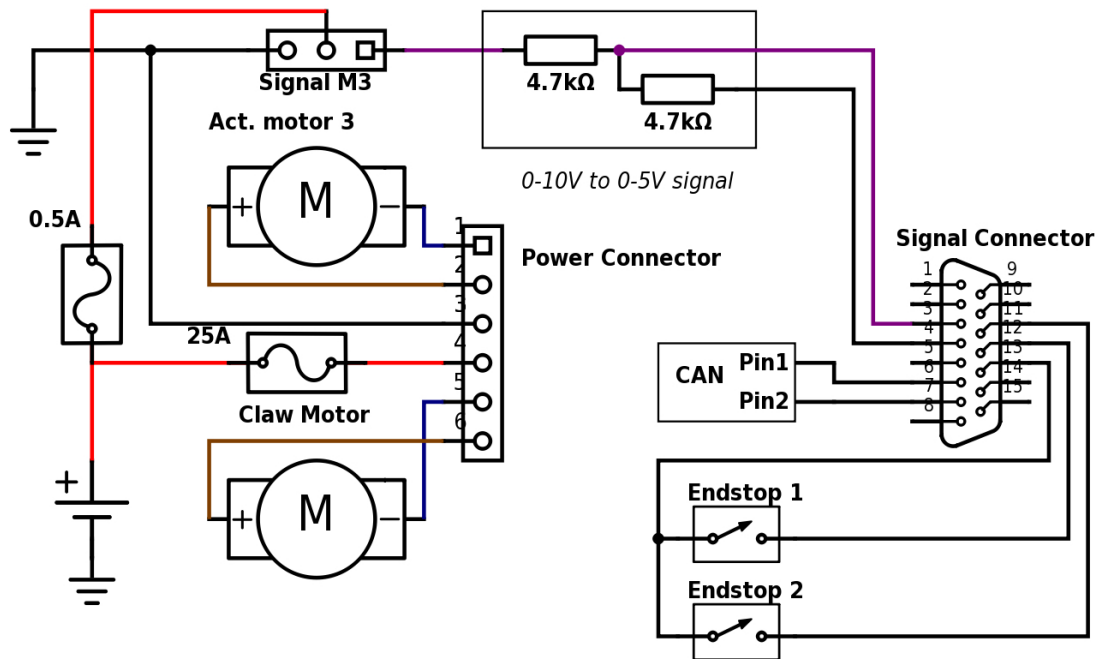


Figure 9.5: Circuit diagram of the end arm link actuator and the claw motor.

9.4 CAN and ROS Integration

As the Thorvald II platform utilizes the CAN network, both motor controllers must be set up to a node on the network in order to communicate with the platform. This should be an easy task, since the Roboteq controllers supports CANopen protocol, the same protocol used on the robot platform. The connection is made through the CAN high and low pins of the controllers connector.

9.5 Loader Position Control

The desired end positions of the motors are calculated by a node in ROS and published to a ROS topic. Another node subscribing to the same topic will send the message to the CANbus, which in turn passed it on to node of the controllers. The controllers must then ensure that the actuators positions corresponds to the set positions. This is done through the absolute position feedback signal from the actuators.

According to the user manual of the LA36, the signal delay is 20ms and the feedback signal error is rated to 0.5%. This mean that the maximum possible error when the actuator is fully extended accounts for $350mm \cdot 0.5\% = 1.75mm$. These error conditions should be sufficiently small for closed loop position control.

Based on the feedback, the motor controller will adjust the position, and ROS gets information on the actual position. The position control communication system is shown

schematically in figure 9.6.

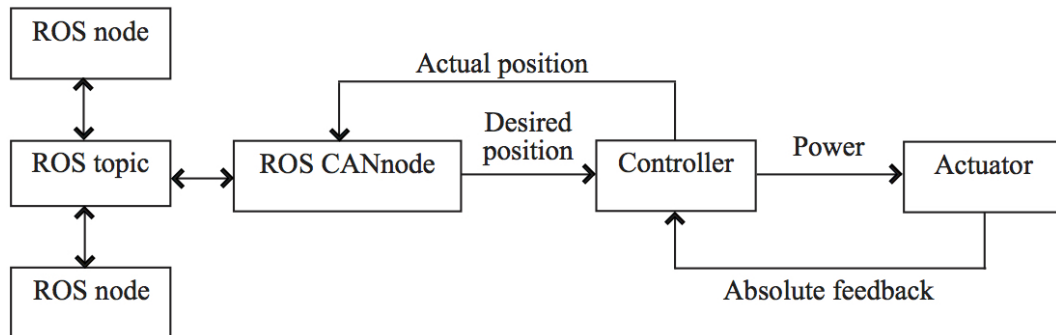


Figure 9.6: Communication network diagram.

9.6 Gripper Control

Similar to the loader position control, the operation of the gripper is also controlled through ROS. The desired position (open or closed) is determined by a node in ROS and published to a topic, before it is sent by a subscribing node to the CANbus, and finally to the node the controller.

The claw motor is set to work on full power until one of the end stop switches is engaged. Depending on which switch is engaged, the controller will know the motor's correct direction of rotation. In order to operate correctly the controller needs a script to verify which switch is engaged at all time. The new status of the gripper is then sent back to ROS.

9.7 Safety

The Norwegian Regulation of Machines [55] requires any machine with a possible crush hazard to have emergency stop switches. Stop switches are already implemented on the robot platform, so the power supply to the transformer of the loader will be wired via those.

Chapter 10

Control Setup

Chapter 10 present the laboratory experiment of matching the Roboteq controller with both actuation components. The experiment involved connecting the motors and controllers correctly before attempting to configure them using the supplied software. The software, Roborun+ enables testing, configuration and script implementation to Roboteq controllers.

The LinAk LA36 actuators are of the most sophisticated electric linear actuators on the market, usually controlled by LinAk's own controllers and software. The Roboteq controllers are generically designed to control brushed electric motors. However, combining the two proved more difficult than expected.

10.1 Controller Setup

Before the testing of the controllers could start, the Roborun+ PC utility software of Roboteq was installed on a stationary computer in the robotics lab.

The SDC2160 controller and a single LA36 actuator were set up (figure 10.1) according to the circuit diagram of figure 9.4, with a laboratory electric converter as the power source. At first, the software could not recognize the connected controller. Several cables and a second controller were tried in different combinations before the PC finally recognized the controller. Once the software found the controller, the input and output parameters were set to analogue feedback input and closed loop position tracking for the motor, according to the manual. The motor responded to the commands and extended the actuator. However, the feedback signal was absent, thus, the motor went on without control. After some fiddling-about with the connections and input parameters, the controller found a feedback signal. Still, there was no change in the signal as the motor operated. The signal problem was further investigated by continuously measuring the signal voltage with a multimeter, as shown in figure 10.1, while running the motor in open loop mode. As expected, the signal corresponded to the actual position of the actuator. This meant that the issue was within the controller or the software.

According to PhD student Lars Grimstad, issues like these are common with Roboteq controllers in general. After once again changing to the other controller, Grimstad gave the advice of updating the firmware. Nonetheless, the problem was still apparent after the update. As a final attempt to solve the issue, an additional voltage reduction-block was soldered to the breakout board in order to use another input channel for the feedback signal. Finally, the controller read the signal and the control loop testing could commence.

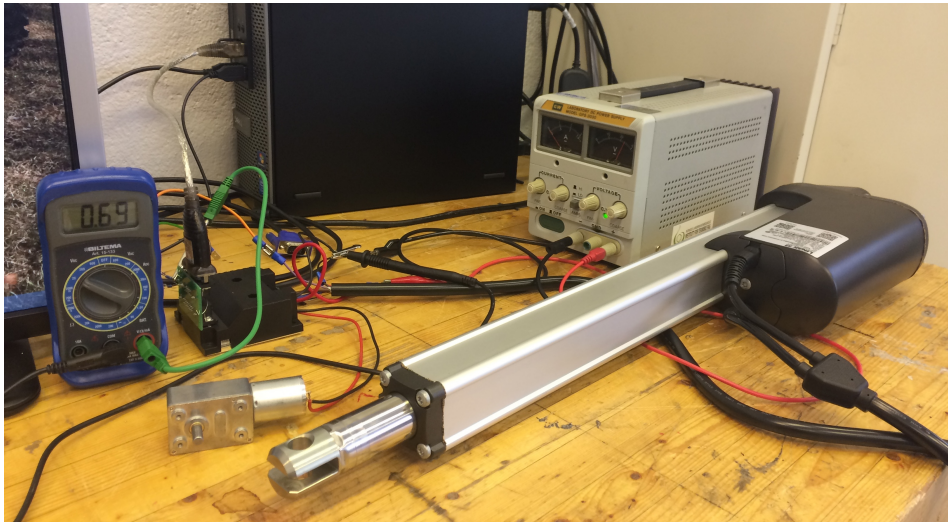


Figure 10.1: Photo of the workbench in the robotics lab.

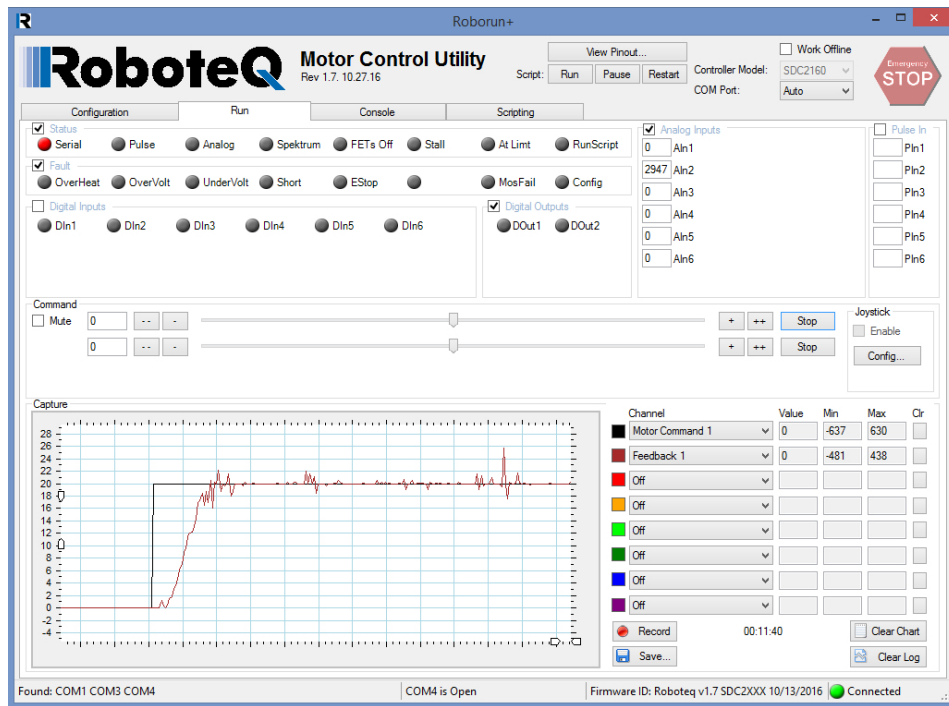


Figure 10.2: Screen-shot of the Roborun+ Utility-program, showing the response of the linear actuator control.

10.2 Actuator Control Loop

In order to tune the control parameters of the system, the motor command set-point is ramped from zero to a desired set point value, and analysing the response of the system. Using Roboteq's default PID parameters in closed loop position tracking mode, the actuator response were an overshoot with declining oscillations around the set point value. After some trial and error adjustments of the PID parameters, the smoothest response was obtained using only the proportional gain. However, once the set point value was reached, the feedback signal was unstable. This caused the motor to oscillate, as it constantly tried to compensate for the relatively small error. As shown in the log chart in figure 10.2, the unstable feedback signal (red line) also had arbitrary pulses of larger errors.

The scale of the problem was attempted reduced by adjusting the *Loop Error Detection* of the controller. This feature stops the motor output channel when a large tracking error is detected over a certain period of time [19]. None of the three available presets would reduce the oscillations. Setting the sensitivity to 250 ms with an error >100 mV immediately stopped the motor upon acceleration, while 500 ms with an error >250 mV or 1s with an error >500 mV made no difference.

Further testing involved changing from motor channel 1 to channel 2, but the problem remained. The problem with the feedback signal also came back. At random moments, the feedback values falls out and remains at zero, despite that the signal is apparent in the analogue input dialog box and on the multimeter.

From this and the troubleshooting in the previous section, the problem with the feedback fallout is most likely within the software or firmware of the controller. Luckily, the signal came back from time to time, at least allowing some further testing to be done. The response of the system when ramping from one set point value to another was improved by adjusting the input deadband from the default 10% to 0%. This parameter select the range of the change in the signal before a new command is given. Setting it to zero will allow a new command to be given immediately when the input signal changes.

Although the continuously rippling signal causes the motors to be constantly engaged, the motion of the actuator is practically stationary because of the backlash in the motor gears. However, it is certainly desirable to let the motor rest once the set-point value is reached, in order to have an efficient and smooth operating system.

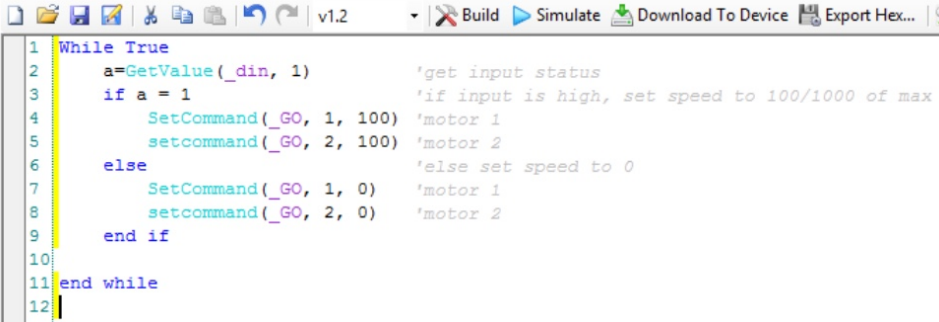
10.3 Gripper Control Loop

In contrast to the configuration of the actuator control, setting up the DC motor for the gripper with the controller went surprisingly easy. After connecting the power leads of the motor to the controller and choosing open loop mode, the motor responded perfectly to the motor commands given in Roborun+.

An end stop switch was connected to the breakout board/connectors according to the power circuit diagram (figure 9.5). The switch broke a 5V signal sent to analogue input 3. The controller recognized the signal and the signal changed on/off according to the switch position.

10.4 Programming the Controllers

The problems concerning the rippled signal described in section 10.2 can be solved by writing a script for the motor controller. By using the MicroBasic scripting abilities of the controllers, they can be programmed to shut off the power of the motors when the desired set point value has been reached. The motors would then rest until the set point command changes. Sadly, there was not enough time to write the suggested script. The script would have a structure similar to the one shown in figure 10.3, and get the value of the position feedback signal, compare it to a criteria and stop the motor if the criteria is true. This applies for control of both the actuators and the DC motor. The difference will be that the actuators utilize numerical feedback and set point values, while the DC motor use on/off feedback and forward/reverse motor commands.



```
1 While True
2   a=GetValue(_din, 1)      'get input status
3   if a = 1                 'if input is high, set speed to 100/1000 of max
4     SetCommand(_GO, 1, 100) 'motor 1
5     setcommand(_GO, 2, 100) 'motor 2
6   else                     'else set speed to 0
7     SetCommand(_GO, 1, 0)  'motor 1
8     setcommand(_GO, 2, 0)  'motor 2
9   end if
10
11end while
12
```

Figure 10.3: A simple MicroBasic script. Courtesy of Grimstad [20].

10.5 Operating Script

The actual motor control script described in the previous section is most practically implemented into the controller. The rest of the operation script, on the other hand, must be scripted and implemented into ROS because the operation and control of the loader mechanism is relative to the operation of the robot.

The foundation for writing an operating script has been discussed in parts throughout both parts of the thesis. The fundamental sequences of the script is shown in the flow diagram of figure 4.2. For each sequence, the operating script must evaluate the actual position of the gripper claws and end effector and command a response accordingly. The control process of the actuators and the gripper is described in section 9.5 and 9.6 respectively.

Discussion Part II

Part II of the thesis concerns subjects of which the author has limited or no formal education. It is therefore important to acknowledge that the work presented might differ from the usual conventions of each subject. As a result of having to spend more obtaining knowledge in Part II compared to Part I, the actual progress of the design was slower than anticipated.

The mathematical modeling was initially supposed to be carried out using the engineering software MATLAB. Modeling the design using this software would for example enable the possibility of changing design parameters during a workspace analysis in order to optimize the design. A mathematical model in MATLAB could have been used for further analysis concerning singularities (several kinematics solutions to one end effector position) and the manipulability of the arm. The workspace analysis shows that the prismatic end link joint is unnecessary long. Reducing the stroke of the end link actuator would compact the assembly and reduce the net weight of the actuator.

The mathematical model was verified by measurements done on the SolidWorks model. Not surprisingly, the results matched. However, during the work with the mathematical modeling it was found that even the slightest decimal round off resulted in relatively large errors in the model. It is therefore most important that the production and assembly of the manufactured part is done with accuracy. The assembly should also be measured and the model updated accordingly.

The choice of transformer was made without an documented assessment mainly because the university is committed to the selected supplier. Within the assortment of the supplier, the chosen transformer was the only component suitable for the application and the proposed spec requirements.

The LinAk LA36 actuators were ordered with a 0-10 V signal. The order was placed before it was discovered that the Roboteq controllers only tolerates a 0-5 V signal input. The problem was fortunately solved by adding a voltage reducing resistor and earth connection. This was, obviously, a glitch that should be avoided in the future.

The goal of reaching level 3 on the TRL scale was obtained by proofing through experiments that the motor controller, the actuator, and DC motor were compatible. Sadly, the experiments did not come far enough to verify the design of the power circuit or the suggested control methods. This was due to the troubles concerning the feedback signal, but also the lack of time to perform more extensive laboratory work. In order to proceed with the work and truly prove the control system the suggested script must be compiled and further experiments conducted. One must therefore conclude that level 3 on the TRL scale is not completely obtained. There was no experimental proof in this thesis of either the CAN network or the setup with ROS. However, these are used through the development of the robot platform and is therefore regarded as validated technologies.

Conclusion Part II

Part II of this thesis aimed to mathematically model the mechanical design presented in Part I and design a control system for the loader implement.

The geometry of the robot arm was modelled mathematically and the inverse kinematics was solved analytically with a unique solution. The kinematic equations will be used in the future implementation of a position control system. A workspace analysis was presented graphically in the same chapter. The analysis showed a potential for optimizing the lengths of the links and the joint variable of the end link to make the arm operate more efficiently.

Two RoboteQ SDC2160 dual-channel motor controllers was chosen to control all four motors of the implement. The control of the joint variables (linear actuators) was set up in closed loop position tracking mode. The gripper control (DC motor) was set up in open loop mode with end stop switches to determine the position of the claws. Laboratory experiments was conducted to match the linear actuators of the arm and the DC motor of the gripper with the motor controller. The experiment revealed issues with the controller firmware and feedback signal noise that need further investigation. The motor controllers communicates with the Robotic Operating System of the robot platform through a Controller Area Network.

Part II of the thesis brought the control system up to level 3 on the TRL scale. This was achieved by analytically proofing the mathematical modeling, electric system, network and communication. Level 3 was further sustained by the laboratory experiments concerning the actuator and motor control.

Future Work

The work of this thesis is only the beginning of the project on utilizing mobile robots in logistical tasks during strawberry harvest. Before the prototype is to be built, the results should be presented for a group with competence in robotics and strawberry production such as the end user (Simen Myhre, possibly other farmers) and the robot research group at NMBU. The group should discuss the presented design and make suggestions for improvements. At the same time, a more complete plan of the entire logistics project, involving robot-human interaction, fleet management, and aspects concerning the humans working alongside of the robot should also be discussed. One should also discuss whether both row environments should be involved in the project, as the loader implement for each of them might benefit from distinctive designs.

As of the prototyping, both operating scripts for the motor controllers and ROS regarding actuator control are the first things that should be worked out. The ROS script should also implement the kinematic equations found in section 7.1 to make a motion/trajectory planning algorithm. The design should also be modelled in ROS using URDF-files and combined with the robot platform model in order to allow computer simulation of the vehicle-manipulator system.

Once the scripting and control system is tested and validated, it makes sense to build the mechanical prototype in order to test its functions and the design. The results of the testing should then be used to suggest improvements of the mechanical design. In a longer term, the implementation of an advanced crate bed system that can hold multiple crates for efficient transport should be assessed.

At the same time, a system regarding machine vision should be elaborated. This involves the steps needed for the robot to locate a crate, approach it and position itself accordingly before the robot arm picks it up. Such a system would need one or more cameras, object recognition algorithms, control algorithms concerning the vehicle-manipulator system, and possibly visual or GPS markers on the crates. Finally, the operation of the system must be made autonomous.

All the technologies needed to compose a complete and autonomous crate handling vehicle-manipulator system are available, it is just a matter of adaption and implementation.

Bibliography

- [1] Definition of Technology Readiness Levels - NASA.
URL: https://esto.nasa.gov/files/trl_definitions.pdf, 2015.
- [2] Robotisering av jordbærkassebæring. Personal email correspondence with Simen Myhre simen@myrhene.no, February 24th, 2017.
- [3] Tarald Rørvik. *Aluminiumskonstruksjoner*. SINTEF Building Research, 1997.
- [4] William Callister et al. *Materials Science and Engineering*. Wiley, 8th edition, 2011.
- [5] Erling F. Bjurbeck. Development of a Crate Loader for the Agricultural Robot Thorvald - TIP300. Technical Report , Norwegian University of Life Sciences, Ås, Norway, December 2016.
- [6] LinAk A/S. *User Manual LinAk Actuator LA36*. , Nordborg, Denmark, 1st edition, 2016.
- [7] Elfa Distrelec, Norway.
URL: <https://www.elfadistrelec.no/>, 2017.
- [8] Carlos Gonzalez. What's the difference between pneumatic, hydraulic, and electrical actuators. *Machine Design*, 2015.
- [9] Illustration of a simple electric motor.
URL: http://en.wikipedia.org/wiki/Image:Electric_motor_cycle_2.png, 2006.
- [10] Tiger Brushless DC motor.
URL: <http://www.getfpv.com/motors/tiger-motor-u10-plus-100kv-u-power-professional-motor.html>, 2017.
- [11] Thompson Linear Actuator.
URL: <http://www.design-engineering.com/wp-content/uploads/2016/02/16-Feb-TH0-linear-actuator-625.jpg>, 2017.
- [12] Inside of a stepper motor.
URL: http://www.robotgear.com.au/Cache/Files/ProductImageOriginals/676_The%20inside%20of%20a%20bipolar%20stepper%20motor.jpg, 2017.
- [13] A selection of Elmo servo motors.
URL: <http://www.elmomc.com/products/pictures/Servo-Motors-Elmo.jpg>, 2017.

- [14] Hot and Cold Rolled Tube and Sections.
URL: http://www.robor.co.za/Hot_Cold_Rolled_Tube-and_Sections, 2015.
- [15] Extruded aluminium profiles.
URL: https://www.pa-international.com.au/pa/images/stories/extrusion_aluminium.jpg, 2017.
- [16] Revolute joint figure, Wikimedia Commons.
URL: https://en.wikipedia.org/wiki/Revolute_joint#/media/File:Revolute_joint.svg, 2009.
- [17] Prismatic joint figure, Wikimedia Commons.
URL: https://en.wikipedia.org/wiki/Prismatic_joint#/media/File:Prismatic_joint.svg, 2009.
- [18] How does an encoder work?, Jurie Wiedemann.
URL: <http://hightechsa.blogspot.no/2012/07/instrumentation-how-does-encoder-work.html>, 2012.
- [19] Inc. Roboteq. *Roboteq SDC2160 data sheet.* , Scottsdale, AZ, USA, 1st edition, 2017.
- [20] Lars Grimstad. Powertrain, Steering and Control Components for the NMBU Agricultural Mobile Robotic Platform. Master's thesis, Norwegian University of Life Sciences, Ås, Norway, 2014.
- [21] Frank Tobe et al. Agricultural robots. Technical Report , Tractica, T1111 Pearl Street, Suite 201 Boulder, CO 80302 USA, 2016.
- [22] Jan Tommy Gravdahl & Kristin Ytterstad Pettersen På l Johan From. *Vehicle-manipulator Systems.* Springer, 1st edition, 2014.
- [23] *Farm robots ready to fill Britain's post-EU labour shortage*, Financial Times, UK.
URL: <https://www.ft.com/content/bee97d2-28ff-11e7-bc4b-5528796fe35c>, April 25. 2017.
- [24] Marius Austad. Powertrain and Steering Modules for the NMBU Agricultural Robot. Master's thesis, Norwegian University of Life Sciences, Ås, Norway, 2016.
- [25] Ø ystein Tå rnes Sund. Chassis Modular Design and Electrical Layout for the NMBU Agricultural Robot Project. Master's thesis, Norwegian University of Life Sciences, Ås, Norway, 2016.
- [26] EARTO. The trl scale as a research and innovation policy tool. *EARTO Recommendations*, ():17, 4 2014.
- [27] Agrobot, SW6010.
URL: <http://www.agrobot.com/products.html>, 2012.
- [28] Atlas - the agile anthropomorphic robot.
URL: http://www.bostondynamics.com/robot_Atlas.html, 2016.
- [29] Shigehiko Hayashi et al. Automation technologies for strawberry harvesting and packing operations in japan. *Journal of Berry Research*, 2013.

- [30] Prof. Dr.-Ing. Konrad Reif et al. *Bosch Automotive Handbook*. Wiley, 9th edition, 2014.
- [31] Robot Platform - Knowledge, learning and reasoning.
URL: <http://www.robotplatform.com/knowledge.html>, 2017.
- [32] Pascal's Principle and Hydraulics.
URL: https://www.grc.nasa.gov/WWW/K-12/WindTunnel/Activities/Pascals_principle.html, 2014.
- [33] Heather Tierney et al. Experimental demonstration of a single-molecule electric motor. *Nature Nanotechnology*, 6:625–629, 9 2011.
- [34] ABB drive system to power Boeing wind tunnel.
URL: <http://www.abb.com/cawp/seitp202/05312e63ad3b53b8c12571fe0052173e.aspx>, 2006.
- [35] Theodore Wildi. *Electric Machines, Drives, and Power Systems*. Pearson Education International, 6th edition, 2006.
- [36] Baldor Motors and Drives. *Servo Control Facts - A Handbook Explaining The Basics of Motion*. Baldor Electric Company, N/A.
- [37] inc maxon precision motors. A comparison of dc linear actuators with dc linear motors, 2016.
- [38] Paul E. Sandin. *Robot Mechanisms and Mechanical Devices Illustrated*. McGraw-Hill Higher Education, 2003.
- [39] Carlos Gonzalez. What's the difference between spur, helical, bevel, and worm gears. *Machine Design*, 2015.
- [40] Society of Robots - Close-up of a SCORBOT's belt drives.
URL: http://static.flickr.com/6029/5968563226_990b5525a7.jpg, 2013.
- [41] Laurens van Lieshout - Harmonic-drive animation.
URL: https://nl.wikipedia.org/wiki/Harmonic_drive#/media/File:Harmonic-drive-explanation.gif, 2008.
- [42] Trammell Hudson - Fifth and sixth joint drive mechanism of a PUMA robot arm.
URL: https://c1.staticflickr.com/4/3715/9346253999_bb47019866_b.jpg, 2013.
- [43] Truck final drive of the 1930s. United Kingdom's Government - Public Domain, 1937.
- [44] John Ballantune John M. Hollerbach, Ian W. Hunter. A comparative analysis of actuator technologies for robotics. *Robotics Review* 2, 1992.
- [45] Russel C. Hibbeler. *Mechanics of Materials*. Pearson, 8th edition, 2011.
- [46] Almar Almar-Næss. *Metalliske materialer*. TAPIR akademisk forlag, 2003.
- [47] Aluminum Alloy Heat Treatment Temper Designations.
URL: <http://www.matweb.com/reference/aluminumtemper.aspx>, 2017.
- [48] Robert L. Norton. *Design of Machinery*. McGraw-Hill Higher Education, 4th edition, 2008.

- [49] Astrup Product Catalogue.
URL: <http://www.astrup.no/Materialer-Produkter/Materialer/Aluminium/Standardprofiler>, 2017.
- [50] Mette Mo Jacobsen. *Produktutvikling*. Fortuna Forlag, 1st edition, 1997.
- [51] Tsuneo Yoshikawa. *Foundations of Robotics - Analysis and Control*. The MIT Press, 1th edition, 1990.
- [52] Xiujuan Li Yi Cao, Ku Lu and Yi Zang. Accurate numerical methods for computing 2d and 3d robot workspace. *INTECH - International Journal of Advanced Robotic Systems*, 8(6):1–13, 8 2011.
- [53] Jan Tommy Gravdahl & Pål Johan From. *Innføring i dynamikk og regulerings-teknikk*. Unpublished, 2013.
- [54] ROS wiki.
URL: <http://wiki.ros.org/ROS/Introduction>, 2014.
- [55] Regulation of Machines, Norwegian Law.
URL: https://lovdata.no/dokument/SF/forskrift/2009-05-20-544#KAPITTEL_6, 2009.



Norges miljø- og biovitenskapelig universitet
Noregs miljø- og biovitenskapelige universitet
Norwegian University of Life Sciences

Postboks 5003
NO-1432 Ås
Norway